Supporting Information for:

Luminescent europium and terbium complexes of dipyridoquinoxaline and dipyridophenazine ligands as photosensitizing antenna: structures and biological perspectives

Srikanth Dasari and Ashis K. Patra*

Department of Chemistry

Indian Institute of Technology Kanpur, Kanpur-208016, Uttar Pradesh, India

Table of Contents:	Page

DNA and BSA binding studies

DNA sensing studies

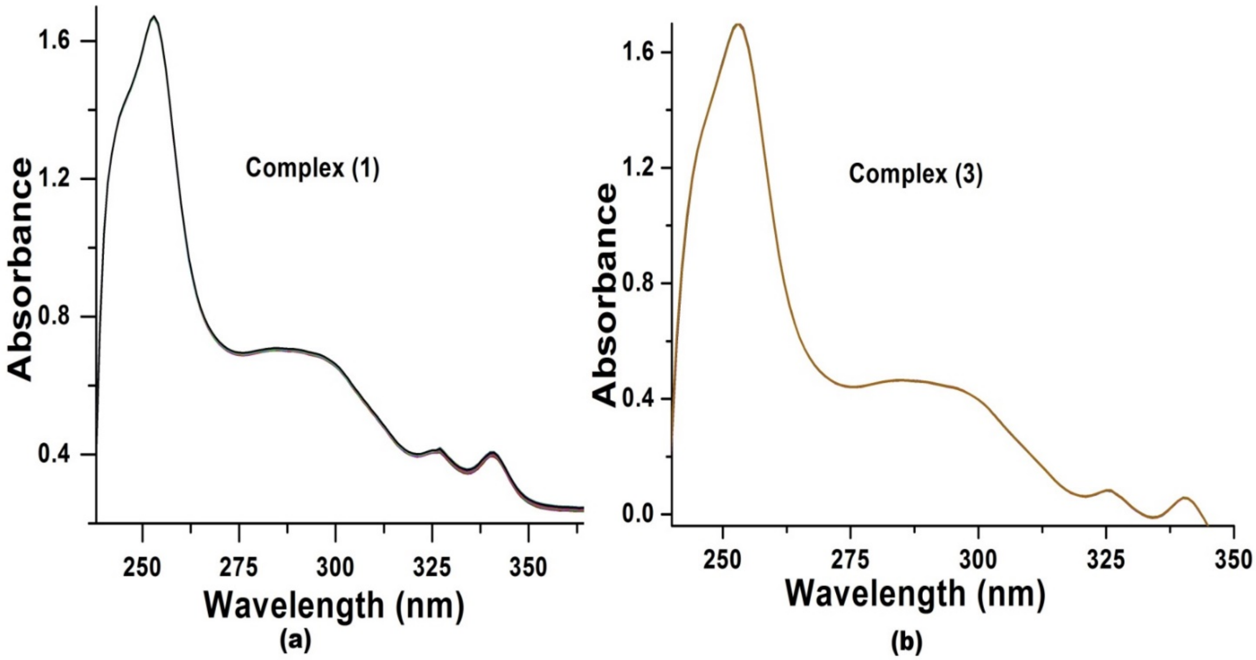

Figure S1: Time-dependent absorption spectral traces of complexes [Eu(dpq)(DMF)$_2$(NO$_3$)$_3$] (**1**) (a) and [Tb(dpq)(DMF)$_2$Cl$_3$] (**3**) (b) monitored for 4 h in DMF at 25 °C to access the stability of the complexes in solution.

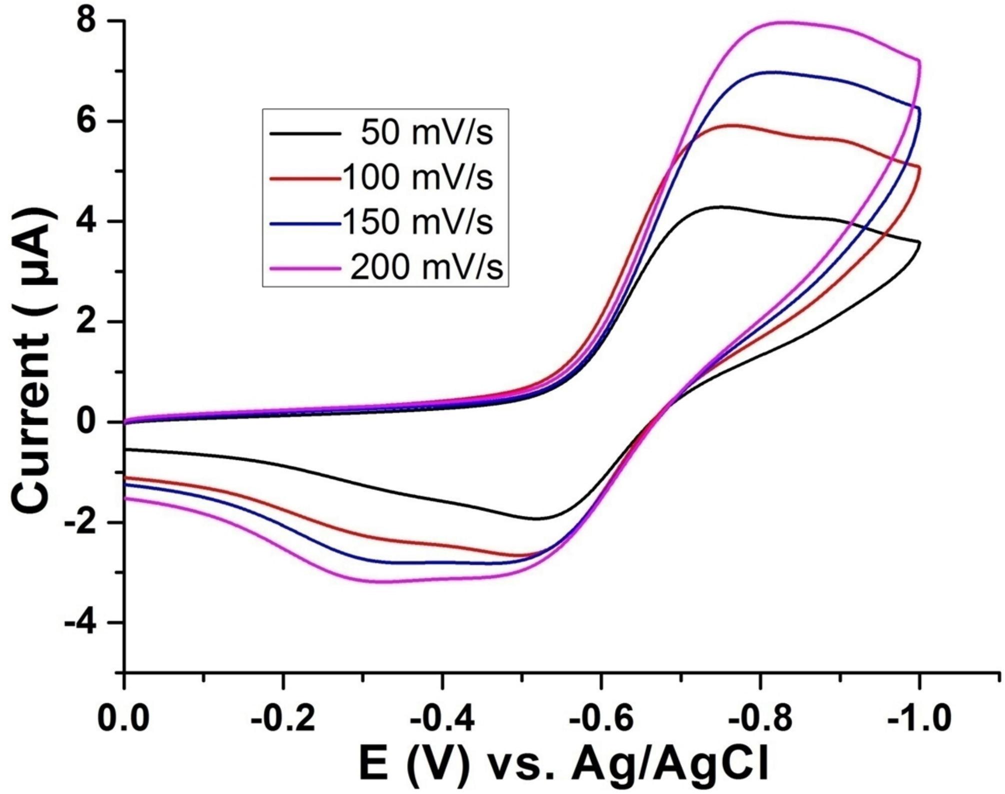

Figure S2. Overlay of cyclic voltammograms of the Eu^{3+} in complex $[Eu(dpq)(NO_3)_3(DMF)_2]$ (**1**) in DMF and 0.1 M tertabutylammonium perchlorate (TBAP) as supporting electrolyte at scan speeds of 50, 100, 150 and 200 mV s^{-1} at 25 °C.

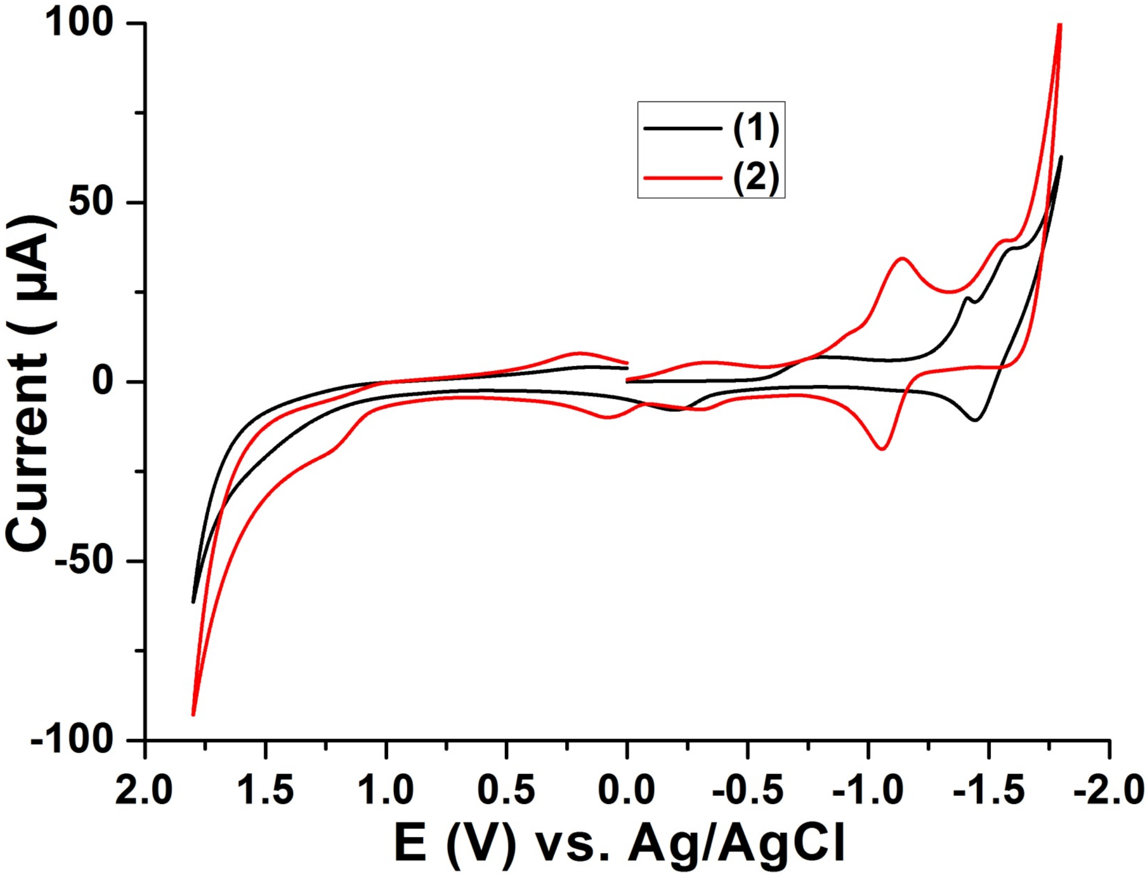

Figure S3. Cyclic voltammograms of the complexes $[Eu(dpq)(DMF)_2(NO_3)_3]$ (**1**) and $[Eu(dppz)_2(NO_3)_3]$ (**2**) in DMF and 0.1 M tertabutylammonium perchlorate (TBAP) as supporting electrolyte at a scan speed of 50 mV s^{-1} 25 °C.

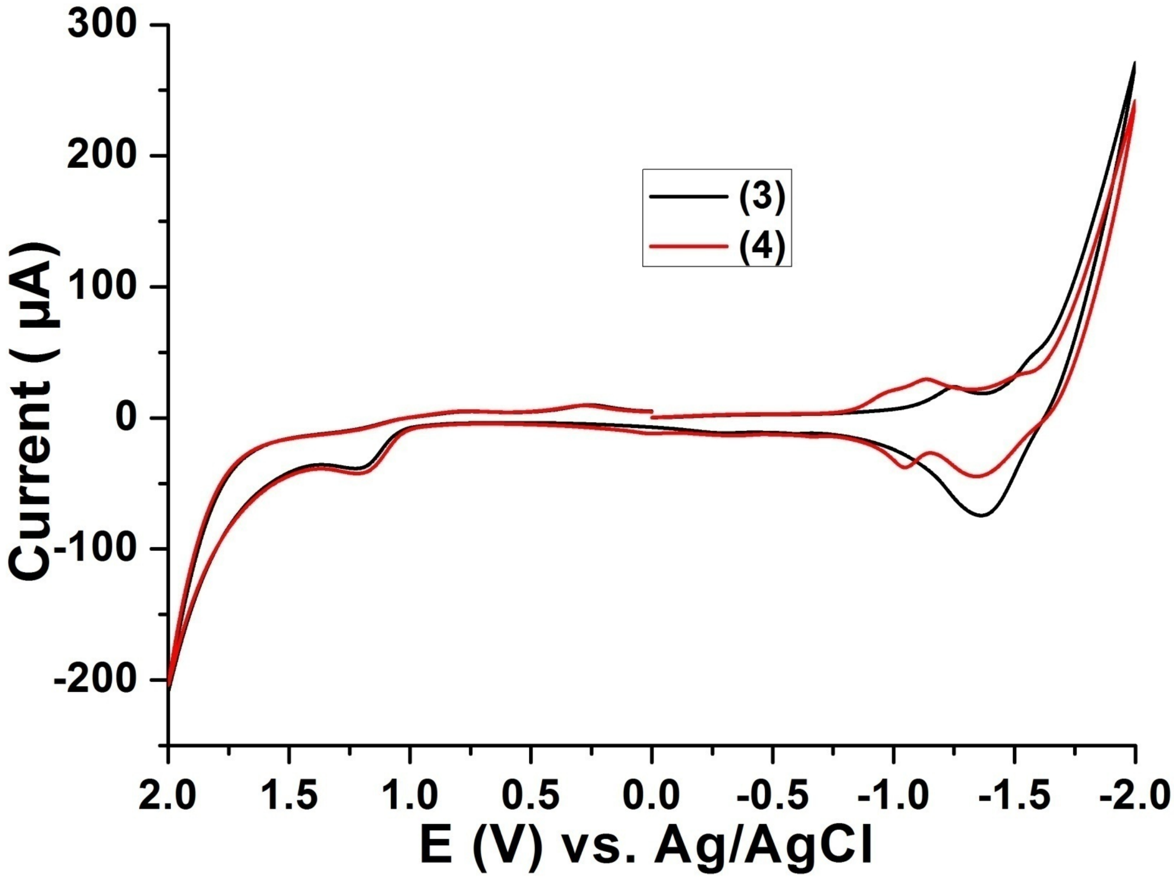

Figure S4. Cyclic voltammograms of the complexes [Tb(dpq)(DMF)$_2$Cl$_3$] (**3**) and [Tb(dppz)(DMF)$_2$Cl$_3$] (**4**) in DMF and 0.1 M tertabutylammonium perchlorate (TBAP) as supporting electrolyte at a scan speed of 50 mV s^{-1} at 25 °C.

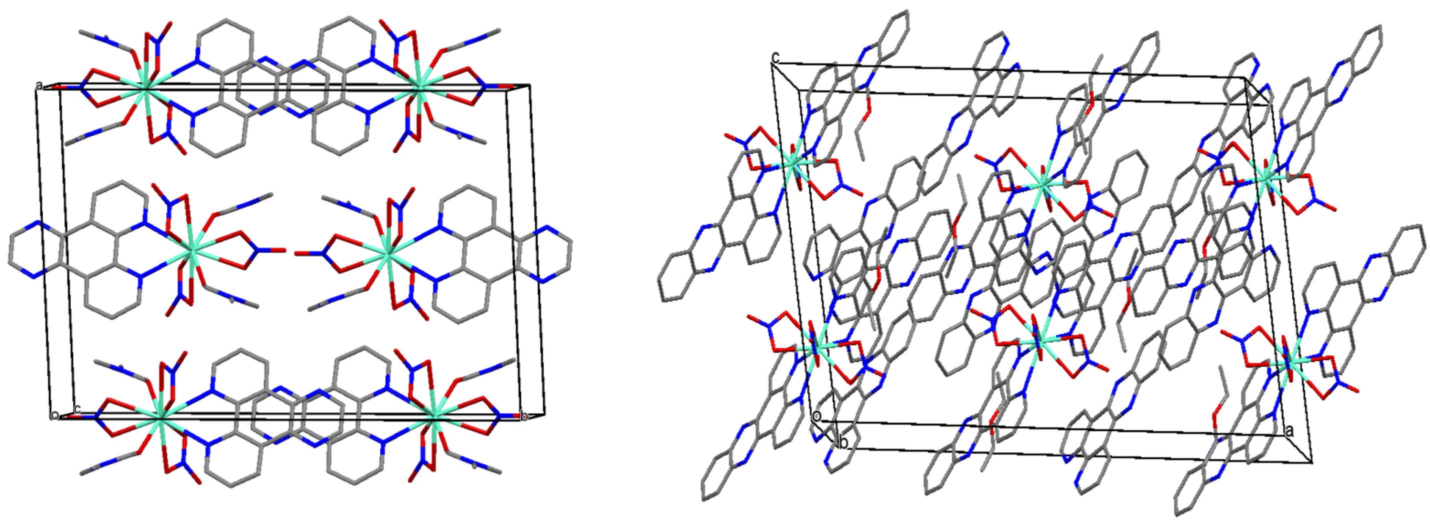

(a) **(b)**

Figure S5. Unit cell packing diagram of complex **1** **(**a**)** and complex **2** (b).

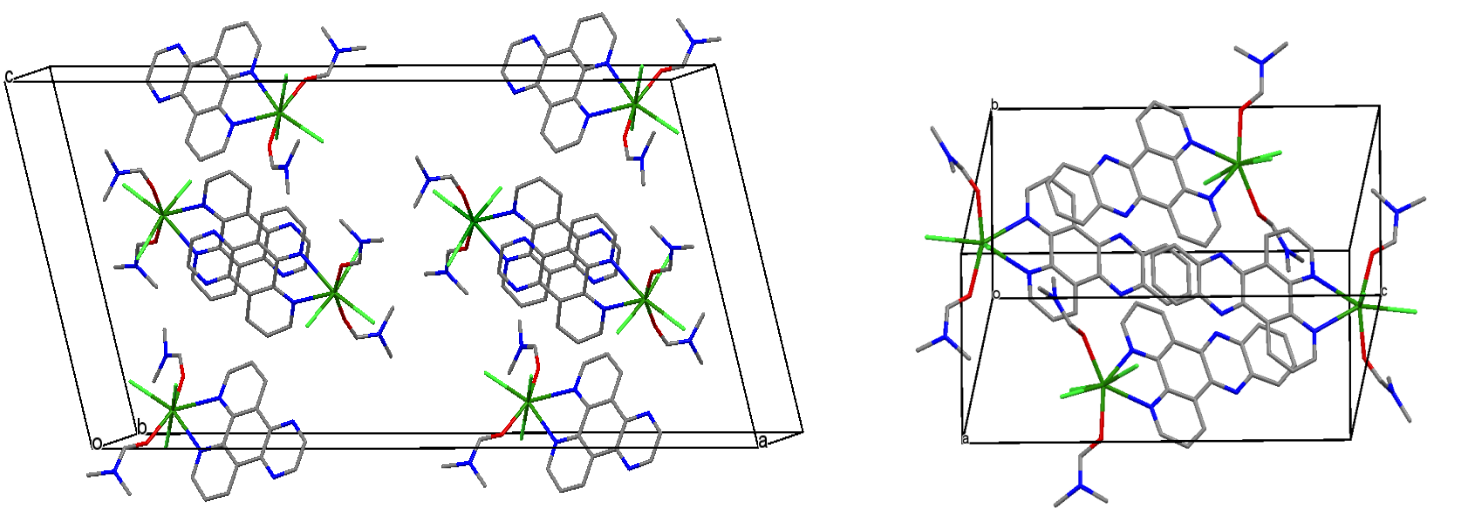

(a) **(b)**

Figure S6. Unit cell packing diagram of complex **3** **(**a**)** and complex **4** (b).

Table S1. Selected crystallographic data and structure refinement parameters for the complexes **1-4**.

Parameters	[Eu(dpq)(DMF)$_2$(NO$_3$)$_3$] **(1)**	[Eu(dppz)$_2$(NO$_3$)]· dppz· Et$_2$O **(2·dppz·Et$_2$O)**	[Tb(dpq)(DMF)$_2$Cl$_3$] **(3)**	[Tb(dppz)(DMF)$_2$Cl$_3$] **(4)**
Empirical formula	$C_{20}H_{22}EuN_9O_{11}$	$C_{80}H_{60}EuN_{19}O_{11}$	$C_{20}H_{22}Cl_3N_6O_2Tb$	$C_{24}H_{24}Cl_3N_6O_2Tb$
M_r	716.43	1615.43	643.71	693.76
crystal system	Monoclinic	Monoclinic	Monoclinic	Triclinic
space group	*C2/c*	*C 2/c*	*C2/c*	*P-1*
a (Å)	15.520(3)	26.496(4)	38.244(8)	7.909(2)
b (Å)	21.290(4)	15.353(4)	7.7857(16)	17.600(5)
c (Å)	8.3672(17)	17.486(4)	17.690(4)	20.746(6)
α (deg)	90.0	90.0	90.0	66.126(5)
β (deg)	109.75(3)	99.482(6)	104.67(3)	84.219(6)
γ (deg)	90.0	90.0	90.0	80.941(6)
Volume (Å^3)	2602.1(9)	7016(3)	5095.5(18)	2605.6(12)
Z	4	4	8	4
D_x (Mg m^{-3})	1.829	1.529	1.678	1.769
μ (mm^{-1})	2.487	0.974	3.118	3.056
F(000)	1424	3296	2528	1368
T (K)	100(2)	100(2)	100(2)	100(2)
θ range for data collection (deg)	1.69 to 25.99°	1.54 to 26.00°	2.67 to 26.00	1.30 to 26.00
Limiting indices	$-19 \le h \le 19$, $-26 \le k \le 26$, $-10 \le l \le 10$	$-32 \le h \le 32$, $-18 \le k \le 18$, $-21 \le l \le 21$	$-39 \le h \le 46$, $-9 \le k \le 9$, $-21 \le l \le 19$	$-9 \le h \le 9$, $-21 \le k \le 21$, $-25 \le l \le 24$
Reflections collected	9861	26586	17445	19998
unique reflections	2535	6892	4974	10038
R(int)	0.0759	0.0600	0.0268	0.0759
T_{max} / T_{min}	0.599 / 0.636	0.9004 / 0.8290	0.604 / 0.574	0.6571/ 0.5801
Data/restraints/parameters	2558 / 0 / 189	6892 / 0 / 504	4974 / 0 / 289	10038 / 0 / 651
GOF on F^2	1.151	1.067	1.122	1.026
R_1[a] and wR_2[b] [$I>2\sigma(I)$]	0.0353, 0.0707	0.0520, 0.1216	0.0238, 0.0660	0.0574, 0.1063
R_1 and wR_2 (all data)	0.0464, 0.0889	0.0759, 0.1445	0.0249, 0.0667	0.1121, 0.1409
Largest diff. peak and hole(e.A^{-3})	2.078 and -1.028	1.513 and -0.819	0.874 and -0.988	1.832 and -1.693

[a]$R_1=\Sigma||F_o|-|F_C||/\Sigma|F_0|$; [b]$wR_2=\{\Sigma[w(F_o^2-F_C^2)]/\Sigma[w(F_0^2)^2]\}^{1/2}$

Table S2: Selected bond lengths (Å) and bond angles (deg) for [Eu(dpq)(DMF)$_2$(NO$_3$)$_3$] (**1**).

Bond lengths (Å)			
Eu(1)-N(1)	2.612(4)	O(6)-Eu(1)-N(1)#1	79.16(12)
Eu(1)-N(1)#1	2.612(4)	O(6)#1-Eu(1)-N(1)#1	137.77(12)
Eu(1)-O(1)	2.492(4)	O(1)#1-Eu(1)-N(1)#1	78.04(13)
Eu(1)-O(1)#1	2.492(4)	O(1)-Eu(1)-N(1)#1	68.95(13)
Eu(1)-O(2)	2.547(4)	O(4)-Eu(1)-N(1)#1	135.11(12)
Eu(1)-O(2)#1	2.547(4)	O(4)#1-Eu(1)-N(1)#1	147.27(12)
Eu(1)-O(4)	2.530(4)	O(2)#1-Eu(1)-N(1)#1	67.53(13)
Eu(1)-O(4)#1	2.530(4)	O(2)-Eu(1)-N(1)#1	106.04(13)
Eu(1)-O(6)	2.361(3)	O(6)-Eu(1)-N(1)	137.77(12)
Eu(1)-O(6)#1	2.361(3)	O(6)#1-Eu(1)-N(1)	79.16(12)
Bond Angles (deg)		O(1)#1-Eu(1)-N(1)	68.95(13)
O(6)-Eu(1)-O(6)#1	142.39(18)	O(1)-Eu(1)-N(1)	78.04(13)
O(6)-Eu(1)-O(1)#1	120.84(13)	O(4)-Eu(1)-N(1)	147.27(12)
O(6)#1-Eu(1)-O(1)#1	72.57(13)	O(4)#1-Eu(1)-N(1)	135.11(12)
O(6)-Eu(1)-O(1)	72.57(13)	O(2)#1-Eu(1)-N(1)	106.04(13)
O(6)#1-Eu(1)-O(1)	120.84(13)	O(2)-Eu(1)-N(1)	67.53(13)
O(1)#1-Eu(1)-O(1)	141.40(19)	N(1)#1-Eu(1)-N(1)	62.11(18)
O(6)-Eu(1)-O(4)	73.26(12)	O(6)-Eu(1)-N(3)#1	96.28(13)
O(6)#1-Eu(1)-O(4)	72.84(12)	O(6)#1-Eu(1)-N(3)#1	93.72(13)
O(1)#1-Eu(1)-O(4)	86.49(13)	O(1)#1-Eu(1)-N(3)#1	24.70(12)
O(1)-Eu(1)-O(4)	131.23(12)	O(1)-Eu(1)-N(3)#1	136.86(12)
O(6)-Eu(1)-O(4)#1	72.84(12)	O(4)-Eu(1)-N(3)#1	80.44(12)
O(6)#1-Eu(1)-O(4)#1	73.26(12)	O(4)#1-Eu(1)-N(3)#1	130.94(12)
O(1)#1-Eu(1)-O(4)#1	131.24(12)	O(2)#1-Eu(1)-N(3)#1	25.77(12)
O(1)-Eu(1)-O(4)#1	86.49(13)	O(2)-Eu(1)-N(3)#1	150.13(12)
O(4)-Eu(1)-O(4)#1	50.51(16)	N(1)#1-Eu(1)-N(3)#1	68.03(12)
O(6)-Eu(1)-O(2)#1	70.77(13)	N(1)-Eu(1)-N(3)#1	84.88(12)
O(6)#1-Eu(1)-O(2)#1	111.67(13)	O(6)-Eu(1)-N(3)	93.73(13)
O(1)#1-Eu(1)-O(2)#1	50.08(13)	O(6)#1-Eu(1)-N(3)	96.28(13)
O(1)-Eu(1)-O(2)#1	126.93(13)	O(1)#1-Eu(1)-N(3)	136.86(12)
O(4)-Eu(1)-O(2)#1	70.22(12)	O(1)-Eu(1)-N(3)	24.70(12)
O(4)#1-Eu(1)-O(2)#1	116.75(12)	O(4)-Eu(1)-N(3)	130.94(11)
O(6)-Eu(1)-O(2)	111.67(13)	O(4)#1-Eu(1)-N(3)	80.44(12)
O(6)#1-Eu(1)-O(2)	70.77(13)	O(2)#1-Eu(1)-N(3)	150.13(12)
O(1)#1-Eu(1)-O(2)	126.93(13)	O(2)-Eu(1)-N(3)	25.76(12)
O(1)-Eu(1)-O(2)	50.08(13)	N(1)#1-Eu(1)-N(3)	84.88(12)
O(4)-Eu(1)-O(2)	116.75(12)	N(1)-Eu(1)-N(3)	68.03(12)
O(4)#1-Eu(1)-O(2)	70.22(12)	N(3)#1-Eu(1)-N(3)	148.62(16)
O(2)#1-Eu(1)-O(2)	172.92(18)		

Symmetry transformations used to generate equivalent atoms in complex **1**: #1 -x+1, y, -z+3/2.

Table S3: Selected Bond Lengths (Å) and Bond Angles (deg) for $[Eu(dppz)_2(NO_3)_3]$·dppz·Et_2O (**2**).

Bond lengths (Å)			
Eu(1)-N(1)	2.573(4)	O(2)-Eu(1)-N(1)	73.32(11)
Eu(1)-N(1)#1	2.573(4)	O(1)#1-Eu(1)-N(1)	102.65(12)
Eu(1)-N(2)	2.590(4)	O(1)-Eu(1)-N(1)	73.49(11)
Eu(1)-N(2)#1	2.590(4)	O(4)-Eu(1)-N(1)	134.04(12)
Eu(1)-O(1)	2.498(4)	O(4)#1-Eu(1)-N(1)	140.46(12)
Eu(1)-O(1)#1	2.498(4)	N(1)#1-Eu(1)-N(1)	71.34(16)
Eu(1)-O(2)	2.495(3)	O(2)#1-Eu(1)-N(2)	116.29(13)
Eu(1)-O(2)#1	2.495(3)	O(2)-Eu(1)-N(2)	66.43(13)
Eu(1)-O(4)	2.504(4)	O(1)#1-Eu(1)-N(2)	68.08(12)
Eu(1)-O(4)#1	2.504(4)	O(1)-Eu(1)-N(2)	111.57(12)
Bond Angles (deg)		O(4)-Eu(1)-N(2)	72.98(12)
O(2)#1-Eu(1)-O(2)	144.70(17)	O(4)#1-Eu(1)-N(2)	114.87(12)
O(2)#1-Eu(1)-O(1)#1	151.44(13)	N(1)#1-Eu(1)-N(2)	109.64(12)
O(2)-Eu(1)-O(1)#1	130.36(12)	N(1)-Eu(1)-N(2)	63.18(12)
O(2)#1-Eu(1)-O(1)	130.36(12)	O(2)#1-Eu(1)-N(2)#1	66.43(13)
O(2)-Eu(1)-O(1)	51.44(13)	O(2)-Eu(1)-N(2)#1	116.29(13)
O(1)#1-Eu(1)-O(1)	175.40(15)	O(1)#1-Eu(1)-N(2)#1	111.57(12)
O(2)#1-Eu(1)-O(4)	70.86(12)	O(1)-Eu(1)-N(2)#1	68.08(12)
O(2)-Eu(1)-O(4)	77.33(13)	O(4)-Eu(1)-N(2)#1	114.87(12)
O(1)#1-Eu(1)-O(4)	71.37(12)	O(4)#1-Eu(1)-N(2)#1	72.98(12)
O(1)-Eu(1)-O(4)	113.07(13)	N(1)#1-Eu(1)-N(2)#1	63.18(12)
O(2)#1-Eu(1)-O(4)#1	77.32(13)	N(1)-Eu(1)-N(2)#1	109.64(12)
O(2)-Eu(1)-O(4)#1	70.87(12)	N(2)-Eu(1)-N(2)#1	171.87(16)
O(1)#1-Eu(1)-O(4)#1	113.07(13)	O(2)#1-Eu(1)-N(6)#1	25.50(12)
O(1)-Eu(1)-O(4)#1	71.37(12)	O(2)-Eu(1)-N(6)#1	143.40(12)
O(4)-Eu(1)-O(4)#1	51.0(2)	O(1)#1-Eu(1)-N(6)#1	25.99(13)
O(2)#1-Eu(1)-N(1)#1	73.32(11)	O(1)-Eu(1)-N(6)#1	155.80(13)
O(2)-Eu(1)-N(1)#1	141.23(12)	O(4)-Eu(1)-N(6)#1	67.87(12)
O(1)#1-Eu(1)-N(1)#1	73.49(11)	O(4)#1-Eu(1)-N(6)#1	94.56(14)
O(1)-Eu(1)-N(1)#1	102.65(12)	N(1)#1-Eu(1)-N(6)#1	72.59(12)
O(4)-Eu(1)-N(1)#1	140.46(12)	N(1)-Eu(1)-N(6)#1	124.52(13)
O(4)#1-Eu(1)-N(1)#1	134.04(12)	N(2)-Eu(1)-N(6)#1	92.08(13)
O(2)#1-Eu(1)-N(1)	141.23(12)	N(2)#1-Eu(1)-N(6)#1	89.26(13)

Symmetry transformations used to generate equivalent atoms in complex **2**:#1 -x+1, y, -z+1/2.

Table S4: Selected Bond Lengths (Å) and Bond Angles (deg) for [Tb(dpq)(DMF)$_2$Cl$_3$] (**3**).

Bond lengths (Å)			
Tb(1)-N(1)	2.572(2)	O(1)-Tb(1)-Cl(1)	85.12(6)
Tb(1)-N(2)	2.630(2)	N(1)-Tb(1)-Cl(1)	89.64(5)
Tb(1)-Cl(1)	2.6338(8)	N(2)-Tb(1)-Cl(1)	74.27(5)
Tb(1)-Cl(2)	2.6779(10)	O(2)-Tb(1)-Cl(3)	88.62(6)
Tb(1)-Cl(3)	2.6511(10)	O(1)-Tb(1)-Cl(3)	80.52(6)
Tb(1)-O(1)	2.346(2)	N(1)-Tb(1)-Cl(3)	81.24(5)
Tb(1)-O(2)	2.277(2)	N(2)-Tb(1)-Cl(3)	111.56(6)
Bond Angles (deg)		Cl(1)-Tb(1)-Cl(3)	164.64(2)
O(2)-Tb(1)-O(1)	156.36(8)	O(2)-Tb(1)-Cl(2)	78.49(6)
O(2)-Tb(1)-N(1)	125.23(8)	O(1)-Tb(1)-Cl(2)	81.95(6)
O(1)-Tb(1)-N(1)	73.99(8)	N(1)-Tb(1)-Cl(2)	155.89(6)
O(2)-Tb(1)-N(2)	72.35(8)	N(2)-Tb(1)-Cl(2)	138.30(5)
O(1)-Tb(1)-N(2)	131.19(8)	Cl(1)-Tb(1)-Cl(2)	86.67(2)
N(1)-Tb(1)-N(2)	62.39(7)	Cl(3)-Tb(1)-Cl(2)	96.61(3)
O(2)-Tb(1)-Cl(1)	106.73(6)		

Table S5: Selected Bond Lengths (Å) and Bond Angles (deg) for [Tb(dppz)(DMF)$_2$Cl$_3$] (**4**).

Molecule 1		**Molecule 2**	
Bond lengths (Å)		**Bond lengths (Å)**	
Tb(1)-N(1)	2.603(7)	Tb(2)-N(7)	2.566(8)
Tb(1)-N(2)	2.582(7)	Tb(2)-N(8)	2.640(8)
Tb(1)-Cl(1)	2.642(2)	Tb(2)-Cl(4)	2.632(3)
Tb(1)-Cl(2)	2.621(3)	Tb(2)-Cl(5)	2.671(3)
Tb(1)-Cl(3)	2.673(3)	Tb(2)-Cl(6)	2.670(3)
Tb(1)-O(1)	2.328(6)	Tb(2)-O(3)	2.367(6)
Tb(1)-O(2)	2.367(6)	Tb(2)-O(4)	2.244(6)
Bond Angles (deg)		**Bond Angles (deg)**	
O(1)-Tb(1)-O(2)	152.0(2)	O(4)-Tb(2)-O(3)	156.7(2)
O(1)-Tb(1)-N(2)	128.9(2)	O(4)-Tb(2)-N(7)	125.6(3)
O(2)-Tb(1)-N(2)	75.8(2)	O(3)-Tb(2)-N(7)	74.6(2)
O(1)-Tb(1)-N(1)	71.9(2)	O(4)-Tb(2)-Cl(4)	102.55(19)
O(2)-Tb(1)-N(1)	136.1(2)	O(3)-Tb(2)-Cl(4)	86.62(17)
N(2)-Tb(1)-N(1)	63.3(2)	N(7)-Tb(2)-Cl(4)	91.93(18)
O(1)-Tb(1)-Cl(2)	107.80(17)	O(4)-Tb(2)-N(8)	71.4(3)
O(2)-Tb(1)-Cl(2)	83.28(17)	O(3)-Tb(2)-N(8)	131.8(2)
N(2)-Tb(1)-Cl(2)	87.92(17)	N(7)-Tb(2)-N(8)	62.2(3)
N(1)-Tb(1)-Cl(2)	80.11(17)	Cl(4)-Tb(2)-N(8)	75.18(18)
O(1)-Tb(1)-Cl(1)	85.75(17)	O(4)-Tb(2)-Cl(6)	78.71(19)
O(2)-Tb(1)-Cl(1)	85.78(17)	O(3)-Tb(2)-Cl(6)	80.01(16)
N(2)-Tb(1)-Cl(1)	81.24(17)	N(7)-Tb(2)-Cl(6)	154.34(19)
N(1)-Tb(1)-Cl(1)	102.32(17)	Cl(4)-Tb(2)-Cl(6)	89.86(8)
Cl(2)-Tb(1)-Cl(1)	166.19(8)	N(8)-Tb(2)-Cl(6)	142.33(19)
O(1)-Tb(1)-Cl(3)	75.42(16)	O(4)-Tb(2)-Cl(5)	92.87(19)
O(2)-Tb(1)-Cl(3)	78.71(16)	O(3)-Tb(2)-Cl(5)	79.12(17)
N(2)-Tb(1)-Cl(3)	154.44(17)	N(7)-Tb(2)-Cl(5)	78.71(18)
N(1)-Tb(1)-Cl(3)	141.61(17)	Cl(4)-Tb(2)-Cl(5)	164.57(9)
Cl(2)-Tb(1)-Cl(3)	91.47(8)	N(8)-Tb(2)-Cl(5)	110.23(18)
Cl(1)-Tb(1)-Cl(3)	94.63(8)	Cl(6)-Tb(2)-Cl(5)	93.38(8)

General discussion on luminescence spectral properties of the complexes 1-4

Eu^{3+} and Tb^{3+} complexes have distinctive narrow emission bands, large Stokes shift with long excited state luminescence lifetimes, typically in the ms range are ideally suitable for time-gated probes in biological medium. Excitation spectra of complexes in DMF demonstrate similar absorbance profiles with λ_{max} = 272 nm (Fig. S7). Time-delayed luminescence studies under phosphorescent mode were performed to avoid rapid short-lived ligand fluorescence. Under this time-gated condition, Ln^{3+} complexes exclusively display typical $f \rightarrow f$ transition based luminescence on excitation at 272 nm (Figs. S8-S10). We have also observed similar spectral profile when excited at longer wavelength of 365 nm. Excitation of Eu^{3+} complexes **1** and **2** leads to characteristic strong red emission in the visible region due to the $^5D_0 \rightarrow ^7F_J$ *f-f* transitions of Eu^{3+} (J = 0-4) and dominated by electric dipole (ED) induced hypersensitive $^5D_0 \rightarrow ^7F_2$ transition. The emission spectra of $[Tb(B)(DMF)_2Cl_3]$ (B= dpq, **3**; dppz, **4**) complexes show characteristic green luminescence assigned to the $^5D_4 \rightarrow ^7F_J$ *f-f* transitions (J = 6-3) of Tb^{3+} (Fig. S8). In complexes **3** and **4**, the $^5D_4 \rightarrow ^7F_5$ transition from excited Tb^{3+} dominates the emission spectra. This clearly demonstrates that photo-excited energy transfer from the dipyridoquinoxaline and dipyridophenazine based light harvesting antenna to the Ln^{3+} is responsible for the indirect population of the luminescent excited states in Eu^{3+} and Tb^{3+} complexes. The excited state lifetimes (τ) were measured from the luminescent decay profiles for the complexes at room temperature. Luminescence lifetime of the complexes ranges from 0.46-0.59 ms in DMF which reduced to 0.17-0.35 ms in water indicating nonradiative quenching via O-H oscillators of lanthanide bound H_2O. Typical decay profiles of complexes **1-4** are shown in Fig. S12-S13 in ESI. The lanthanide complexes exhibit higher overall quantum yield (ϕ = 0.16-0.38) in DMF than in water ((ϕ = 0.06-0.08) due to nonradiative quenching process via O-H oscillators of lanthanide bound H_2O in aqueous media.

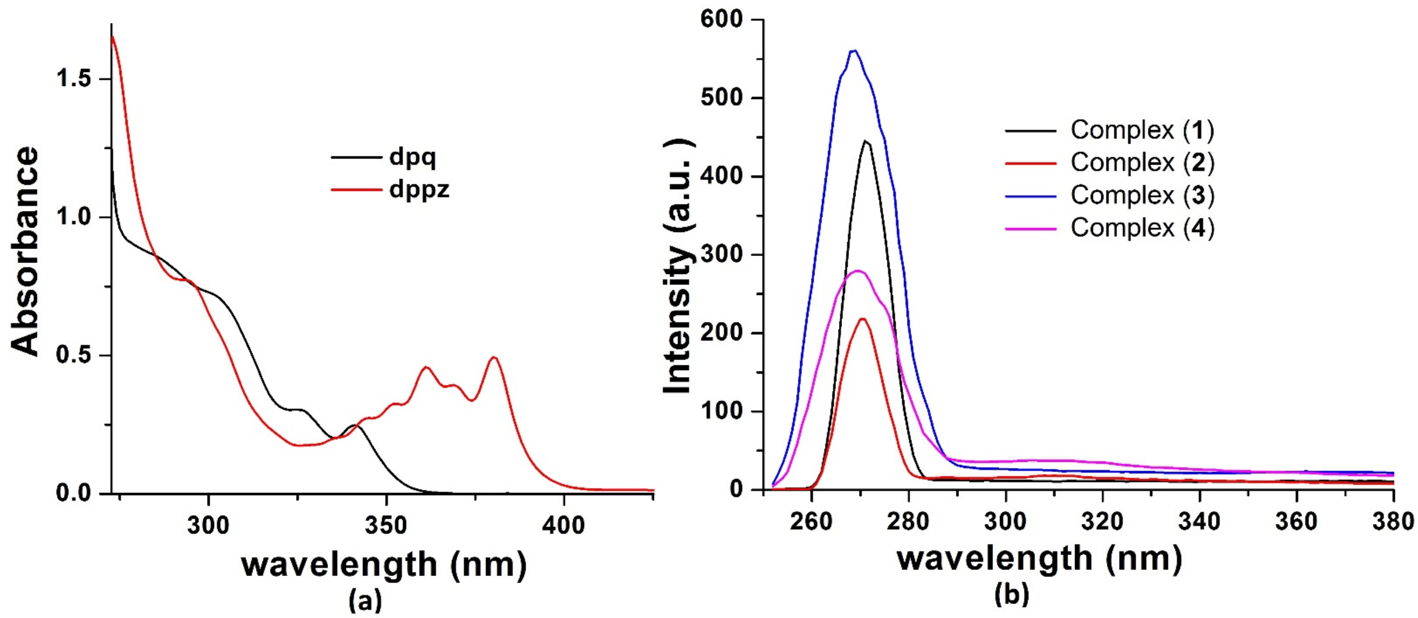

Figure S7. (a) UV-visible spectra of dpq and dppz in DMF. (b) Excitation spectra of the complexes **1-4** in DMF in at 298 K. Excitation and emission slit width = 10 nm, λ_{em} = 616 nm for complexes **1** and **2** and λ_{em} = 545 nm for complexes **3** and **4**.

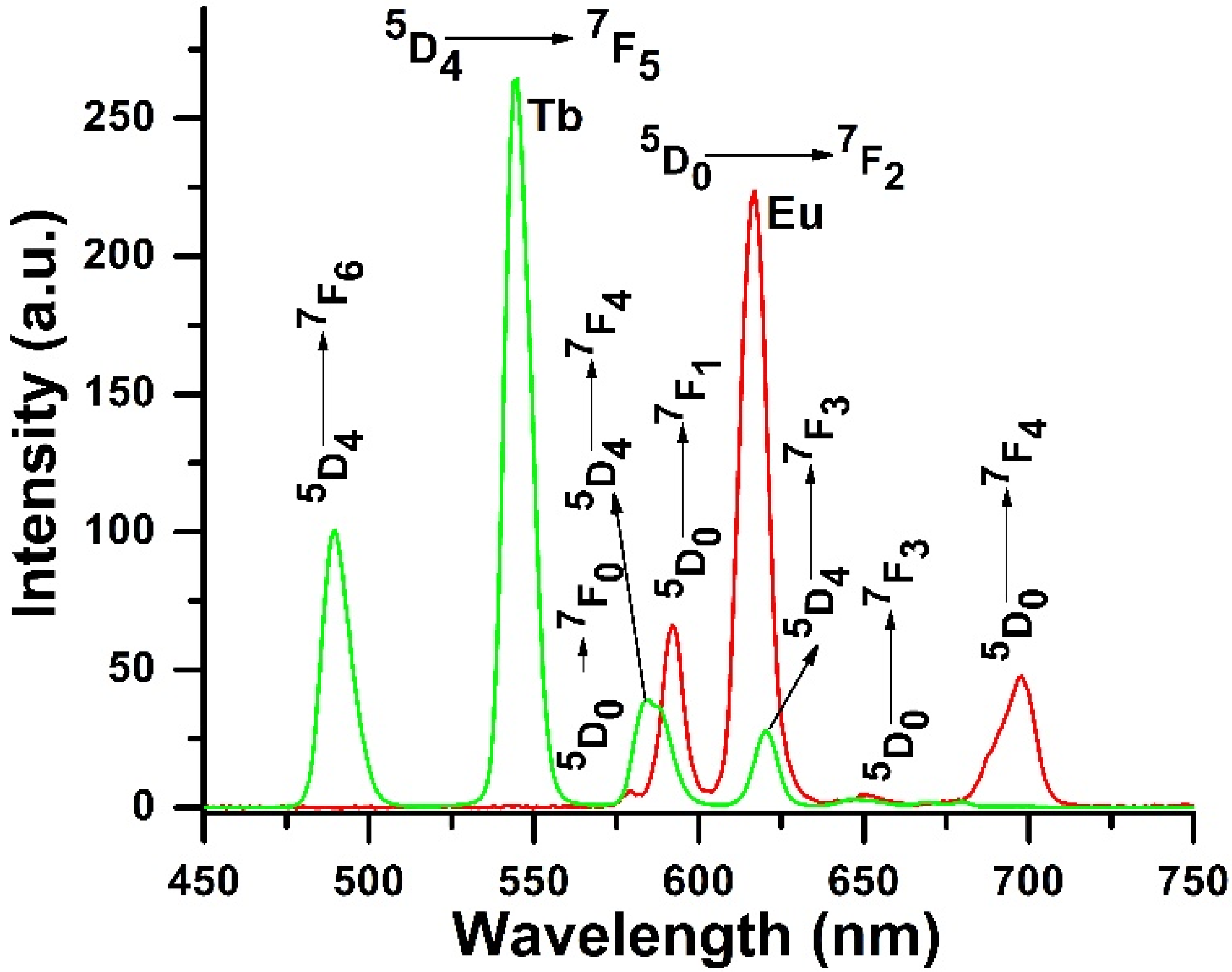

Figure S8. Time-delayed luminescence spectra of $[Eu(dpq)(DMF)_2(NO_3)_3]$ (**1**) (red) and $[Tb(dpq)(DMF)_2Cl_3]$ (**3**) (green) in DMF (delay time = 0.1 ms, λ_{ex} = 272 nm). The corresponding $^5D_0 \rightarrow ^7F_J$ and $^5D_4 \rightarrow ^7F_J$ transitions are shown on the respective spectra.

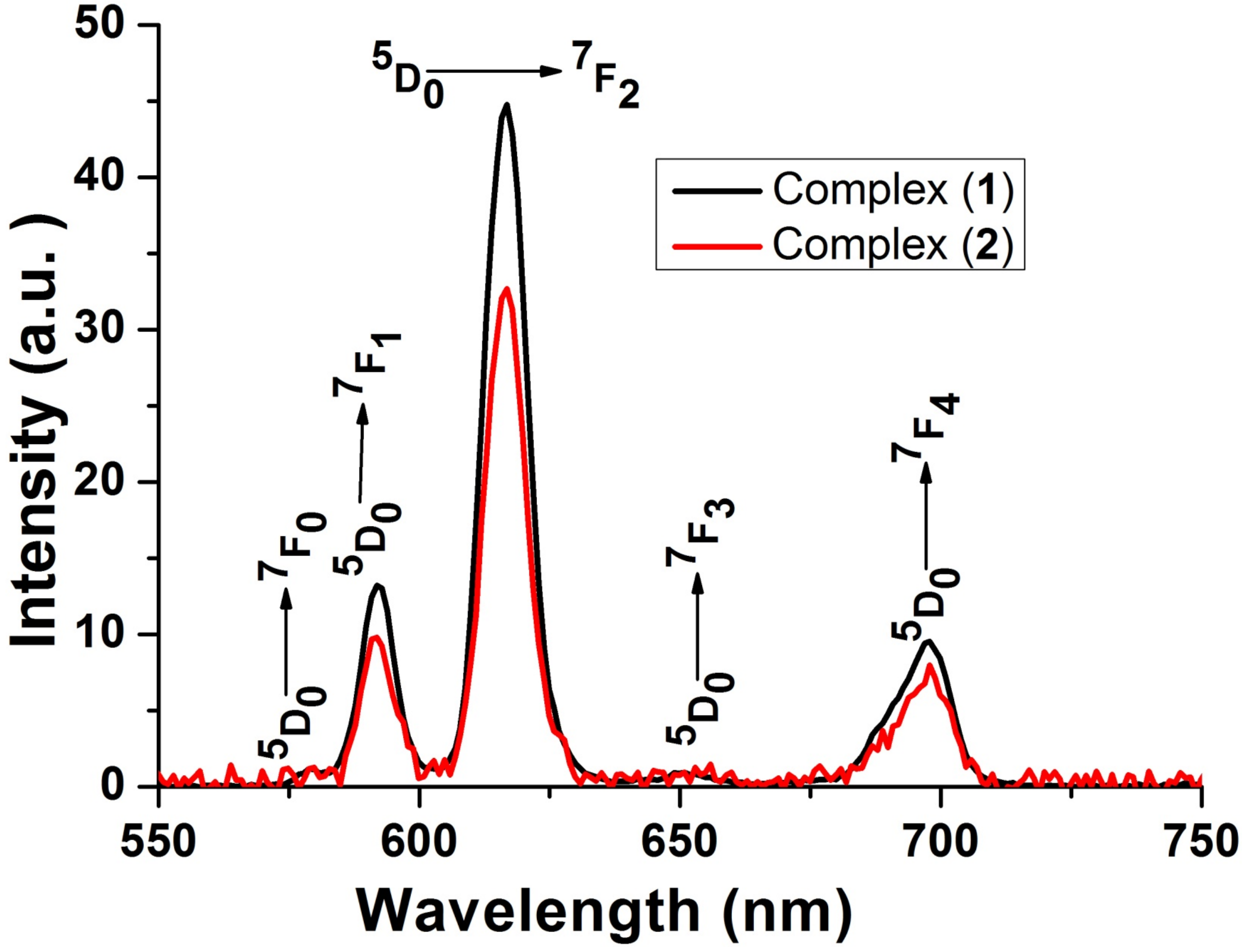

Figure S9. Time-delayed emission spectra of the complexes **1** (black) and **2** (red) (444 μM) in DMF with an excitation at 272 nm (excitation slit width = 5 nm and emission slit width = 5 nm) at 25 °C. Corresponding $^5D_0 \rightarrow {}^7F_J$ transitions are shown on the respective peaks.

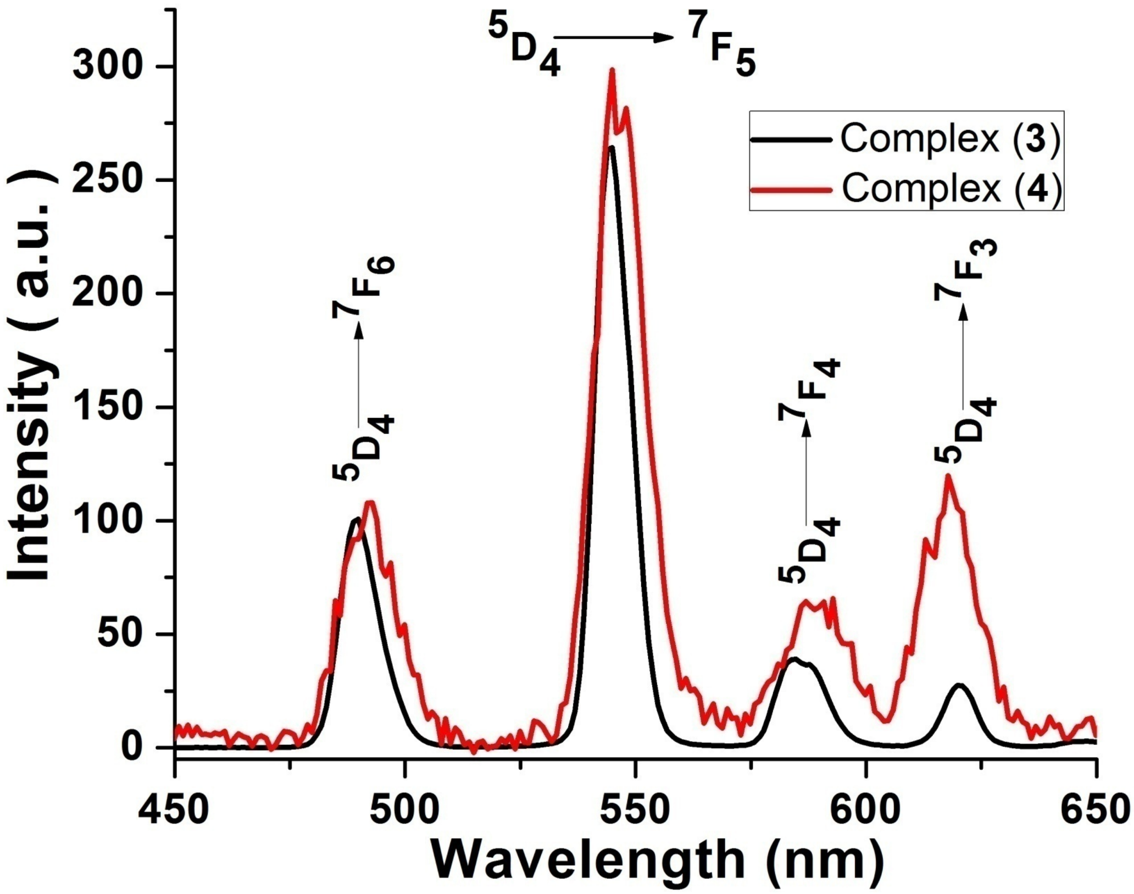

Figure S10. Time-delayed emission spectra of the complexes **3** (black) and **4** (red) (444 μM) in DMF with an excitation at 272 nm (excitation slit width = 5 nm and emission slit width = 5 nm) at 25 °C. Corresponding $^5D_4 \rightarrow {}^7F_J$ transitions are shown on the respective peaks.

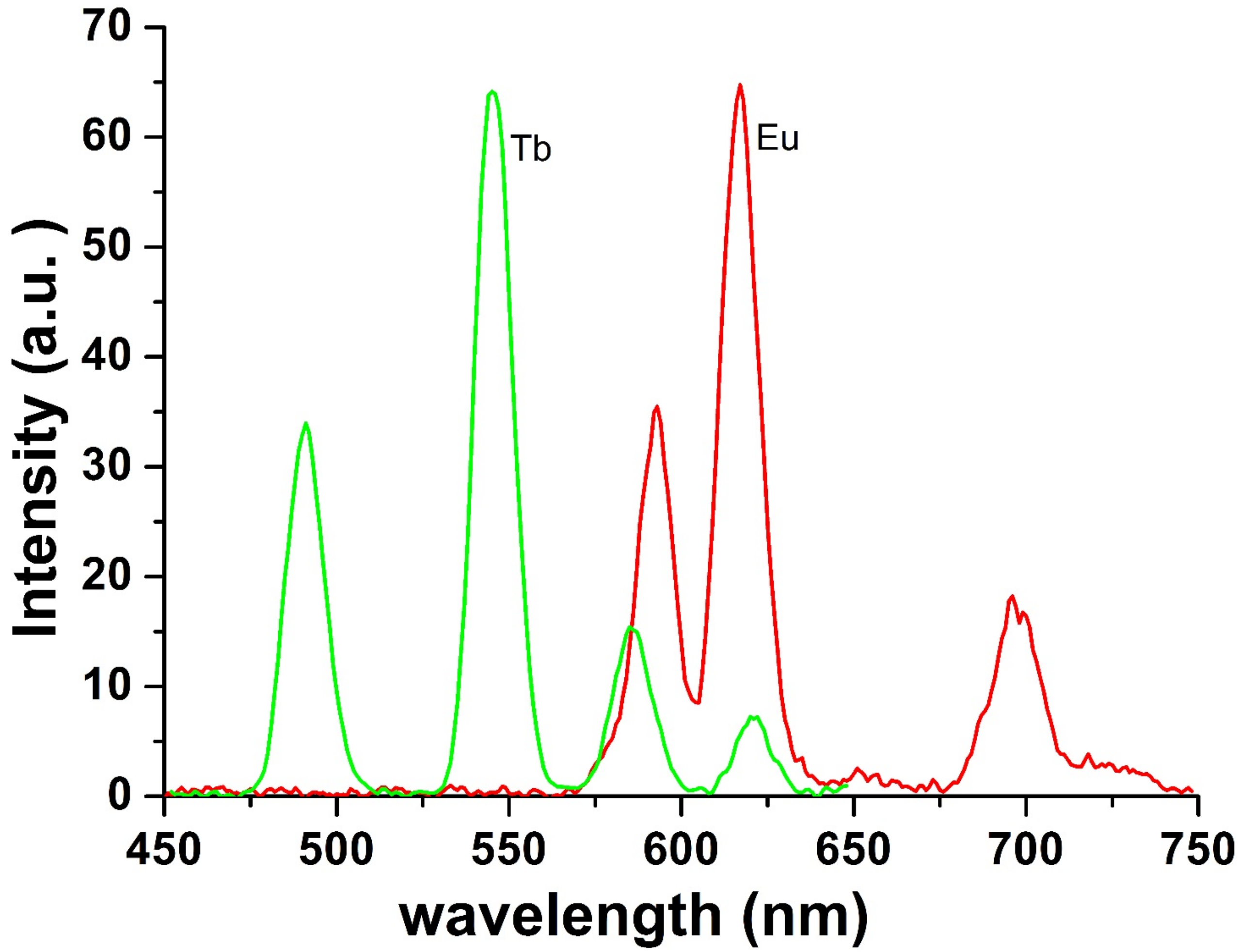

Figure S11. Time-delayed luminescence spectra of [Eu(dpq)(DMF)$_2$(NO$_3$)$_3$] (**1**) (red) and [Tb(dpq)(DMF)$_2$Cl$_3$] (**3**) (green) in DMF (delay time = 0.1 ms, λ_{ex} = 365 nm).

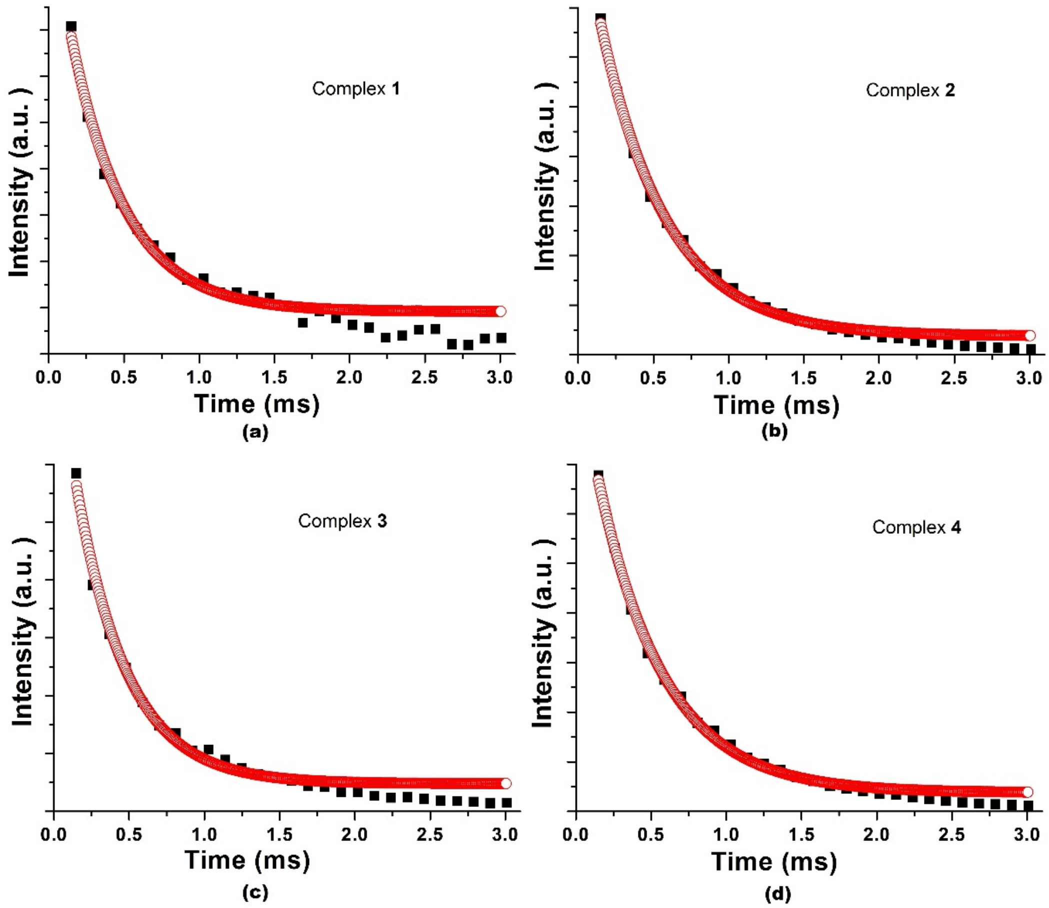

Figure S12. Luminescence decay profile from $^5D_0$ and $^5D_4$ states and lifetime measurements at 616 nm and 545 nm for Eu^{3+} and Tb^{3+} in complexes **1–4** respectively in DMF under ambient condition at 298 K. λ_{ex}= 272 nm, [complex] = 16 μM, delay time and gate time = 0.1 ms, total decay time = 3.0 ms, Ex. and Em. Slit = 10 nm. The red curves are the best fits considering single-exponential behaviour of the decay.

The lifetime (τ) and overall quantum yield ($\Phi_{overall}$) of the complexes listed below.[a]

Complex	τ_{DMF} (ms)	$\Phi_{overall}$[b]
1	0.467	0.325
2	0.492	0.385
3	0.478	0.163
4	0.592	0.161

[a]Quinine sulphate was used as a standard for quantum yield calculation. [b]Quantum yield measurements were done in DMF and within an experimental error of ±10%.

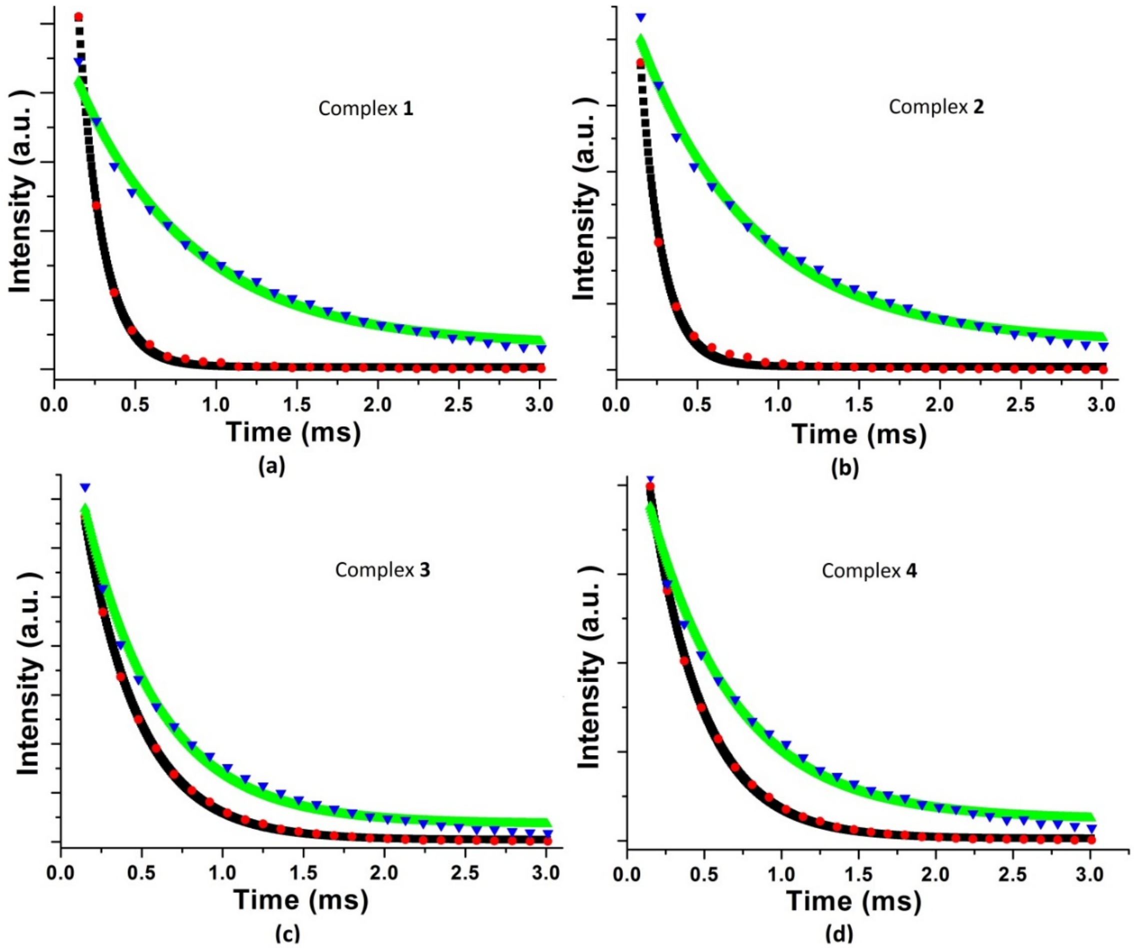

Figure S13. Luminescence decay profile from $^5D_0$ and $^5D_4$ states and lifetime measurements at 616 nm and 545 nm for Eu^{3+} and Tb^{3+} in complexes **1–4** (a, b, c, and d) respectively in H_2O and D_2O under ambient condition at 298 K. λ_{ex}= 272 nm, [complex] = 16 μM, delay time and gate time = 0.1 ms, total decay time = 3.0 ms, Ex. and Em. Slit = 10 nm. The black (in H_2O) and green (in D_2O) curves are the best fits considering single-exponential behaviour of the decay.

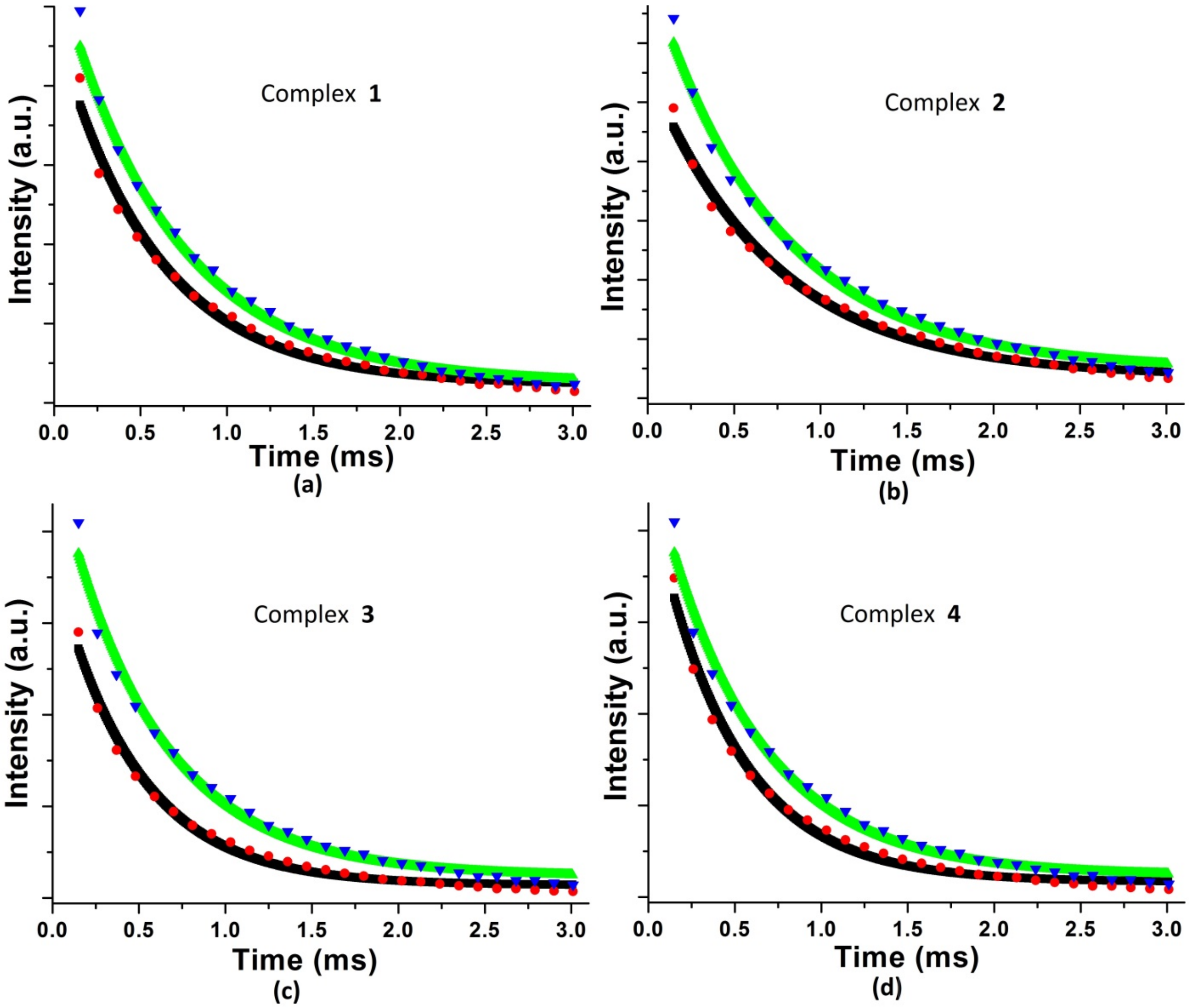

Figure S14. Luminescence decay profile from $^5D_0$ and $^5D_4$ states and lifetime measurements at 616 nm and 545 nm for Eu^{3+} and Tb^{3+} in complexes **1–4** in the presence of CT-DNA (a, b, c, and d) respectively in 5 mM Tris-HCl/NaCl buffer in Milli-Q water (pH 7.2) and in 5 mM Tris-HCl/NaCl buffer in D_2O under ambient condition at 298 K. λ_{ex}= 272 nm, [complex] = 16 μM, [DNA] = 50 μM, delay time and gate time = 0.1 ms, total decay time = 3.0 ms, Ex. and Em. Slit = 10 nm. The black (in Tris-buffer) and green (in Tris-D_2O) curves are the best fits considering single-exponential behavior of the decay.

Table S6. Luminescence lifetime (τ)[a], determination of inner-sphere hydration number (q)[b] and overall quantum yield ($\phi_{overall}$)[c] of the complexes in H_2O and D_2O.

Complex	λ_{ex} (nm)	τ^{H_2O} (ms)	τ^{D_2O} (ms)	q	ϕ^{H_2O}	ϕ^{D_2O}
1	272	0.185	0.720	4.56	0.081 0.037 (365 nm)	0.565 0.292 (365 nm)
2	272	0.176	0.701	4.81	0.066 0.054 (365 nm)	0.575 0.359 (365 nm)
3	272	0.348	0.633	6.16	0.082 0.038 (365 nm)	0.710 0.318 (365 nm)
4	272	0.356	0.696	6.56	0.072 0.059 (365 nm)	0.611 0.415 (365 nm)
4[d]	272	0.353 (aerated) 0.667 (degassed)				

[a]Luminescence lifetime measured from decay profile from $^5D_0$ and $^5D_4$ excited states at 616 nm and 545 nm for Eu^{3+} and Tb^{3+} complexes respectively within experimental uncertainty of ±10%. [b]q is the number of water molecules coordinated to Ln^{3+} ion in solution measured from modified Horrock's equation[42] described in experimental section of manuscript. [c]Quinine sulphate was used as a standard for quantum yield calculation, quantum yields value at λ_{ex} = 365 nm were also mentioned, values are within an experimental uncertainty of ±15%. [d] Lifetime measurements of complex **4** under aerated and degassed condition.

Table S7. Luminescence lifetime (τ)[a], determination of inner-sphere hydration number (q) in presence of CT-DNA.[a]

Complex	λ_{ex} (nm)	$\tau_{\text{Tris buffer in } H_2O}$ (ms)[b]	$\tau_{\text{Tris bufer in } D_2O}$ (ms)[c]	q
1	272	0.546	0.796	0.39
2	272	0.537	0.782	0.40
3	272	0.596	0.701	0.95
4	272	0.606	0.713	0.93

[a][complex] = 16 μM, [DNA] = 50 μM, [b]In 5 mM Tris-HCl/NaCl buffer in Milli-Q water (pH 7.2). [c]In 5 mM Tris-HCl/NaCl buffer in D_2O.

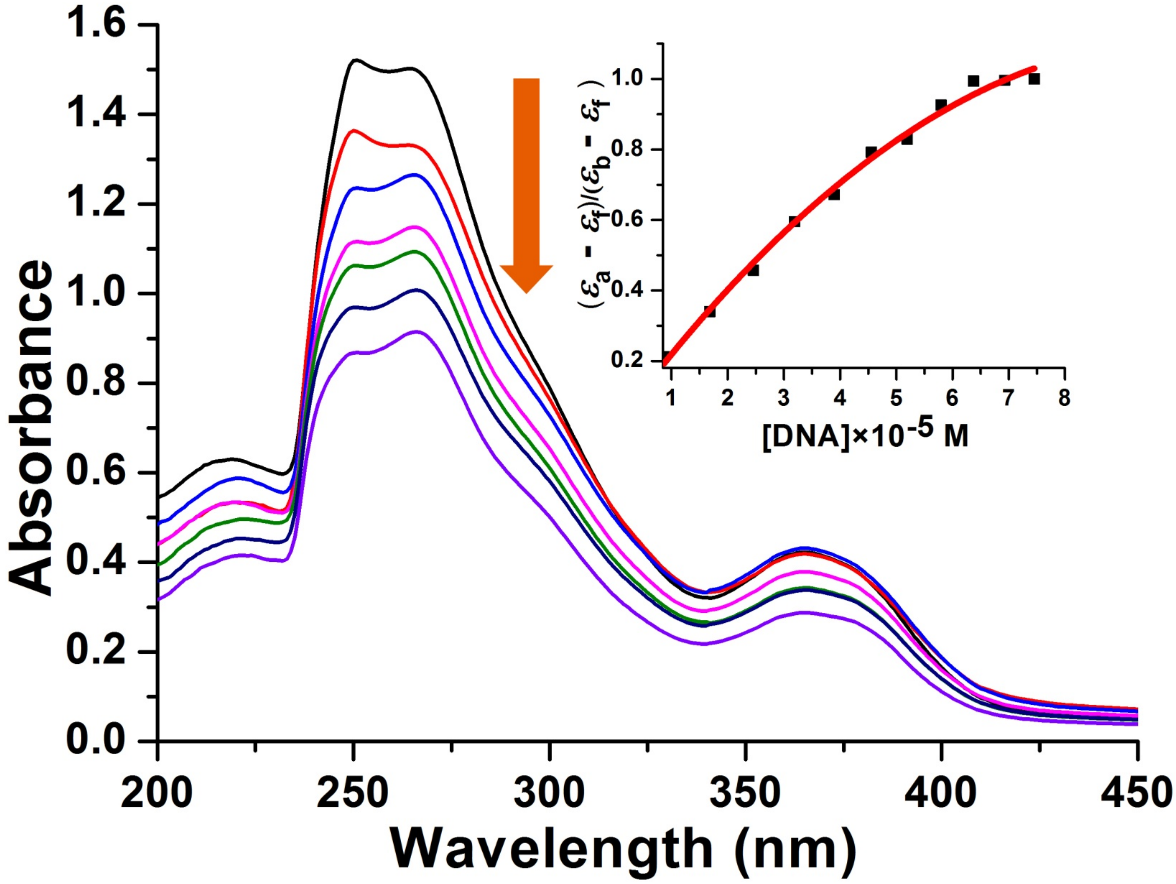

Figure 15. Absorption spectral traces of complex **2** in 5 mM Tris- HCl buffer (pH 7.2) with increasing the concentration of CT-DNA. Inset shows the plot of $\Delta\varepsilon_{af}/\ \Delta\varepsilon_{bf}$ vs. [DNA].

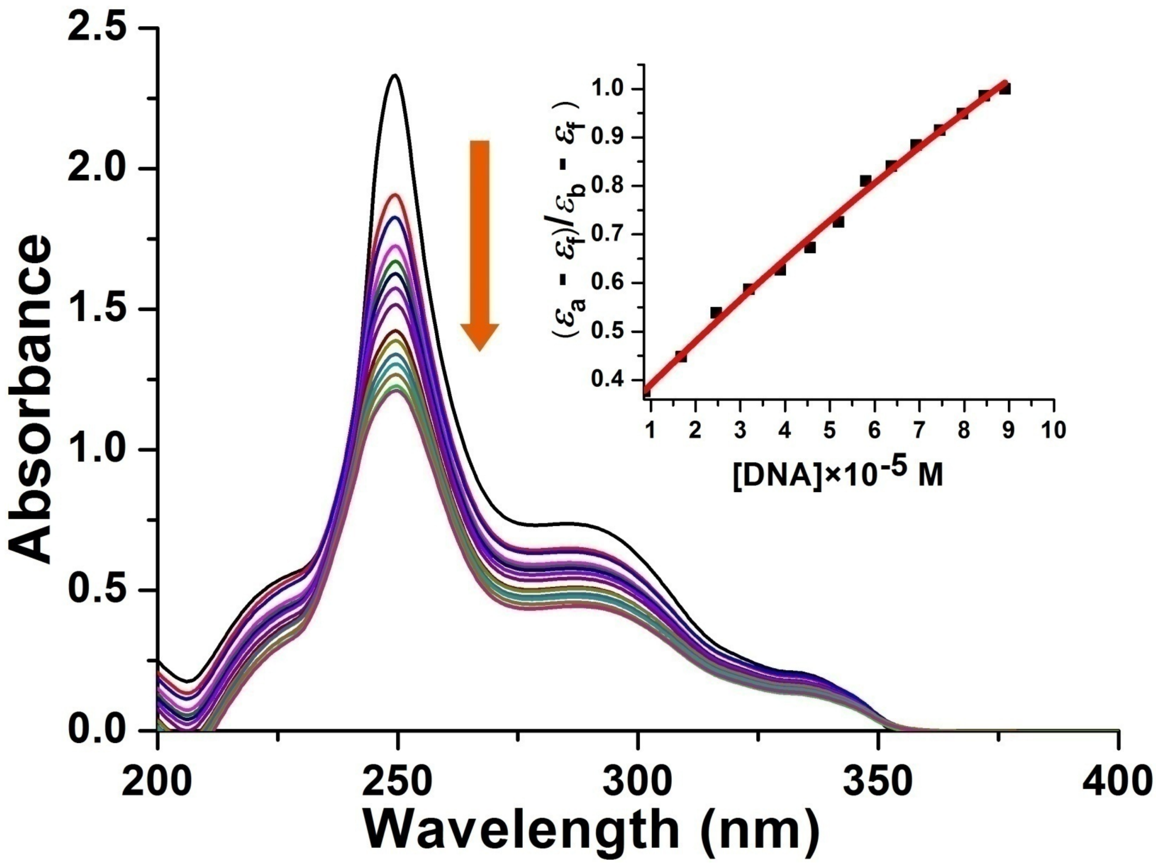

Figure S16. Absorption spectral traces of complex **3** in 5 mM Tris- HCl buffer (pH 7.2) with increasing the concentration of CT-DNA. Inset shows the plot of $\Delta\varepsilon_{af}/\Delta\varepsilon_{bf}$ vs. [DNA].

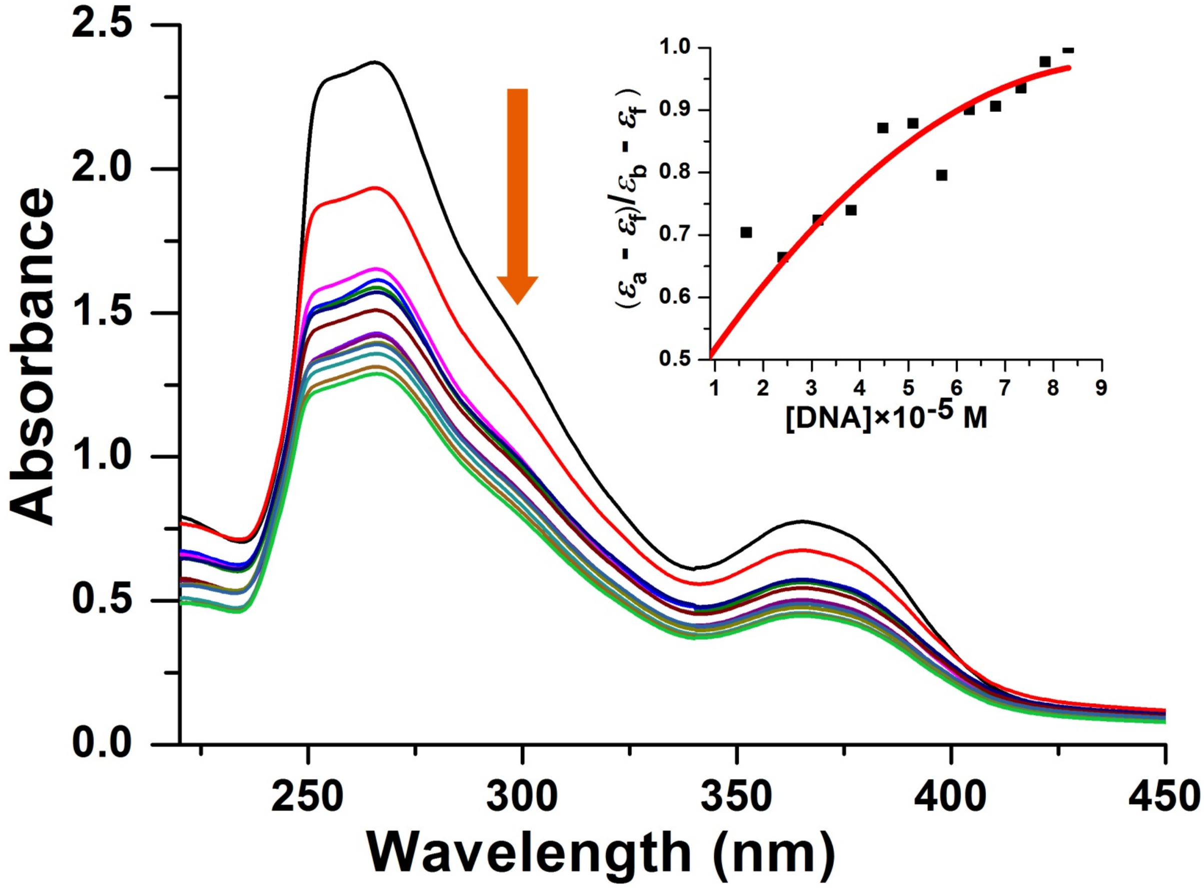

Figure S17. Absorption spectral traces of complex **2** in 5 mM Tris- HCl buffer (pH 7.2) with increasing the concentration of CT-DNA. Inset shows the plot of $\Delta\varepsilon_{af}$/ $\Delta\varepsilon_{bf}$ vs. [DNA].

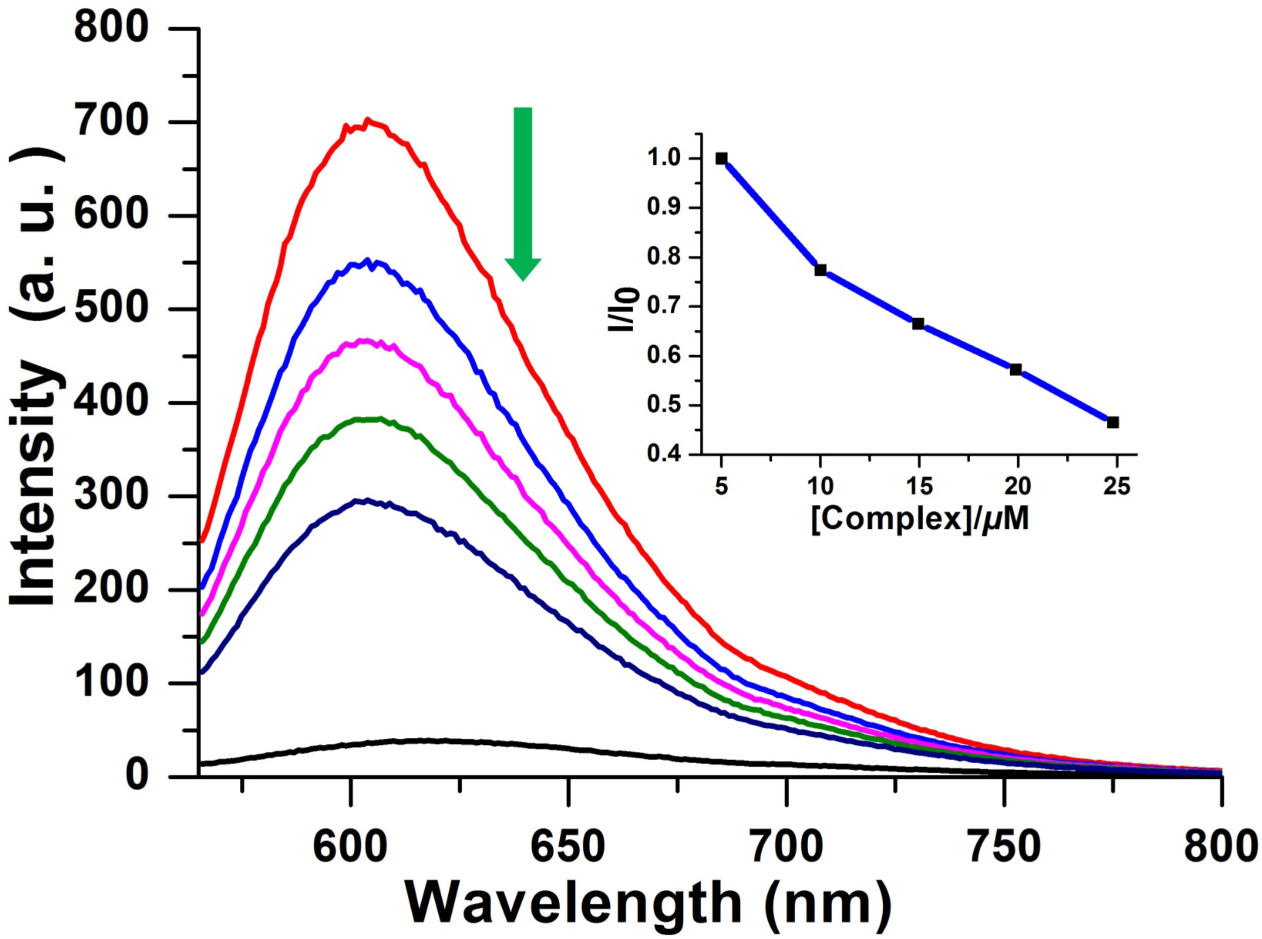

Figure S18. Emission spectral traces of ethidium bromide bound CT-DNA with varying concentration of complex **2** in 5 mM Tris buffer (5 mM Tris-HCl + 5 mM NaCl, pH 7.2) at 25 °C. λ_{ex} = 546 nm, λ_{em} = 603 nm. The inset shows the plot of I/I_0 versus [complex].

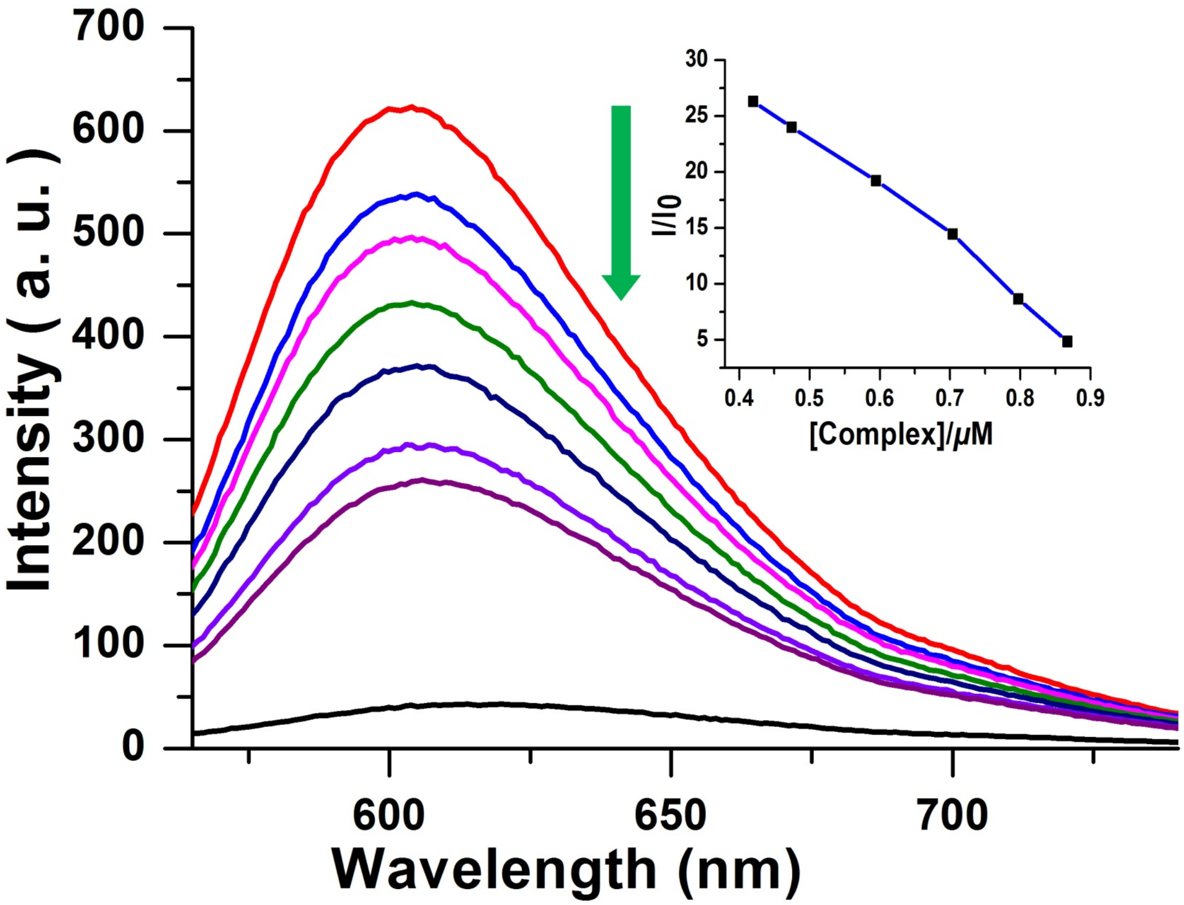

Figure S19. Emission spectral traces of ethidium bromide bound CT-DNA with varying concentration of complex **3** in 5 mM Tris buffer (5 mM Tris-HCl + 5 mM NaCl, pH 7.2) at 25 °C. λ_{ex} = 546 nm, λ_{em} = 603 nm. The inset shows the plot of I/I_0 versus [complex].

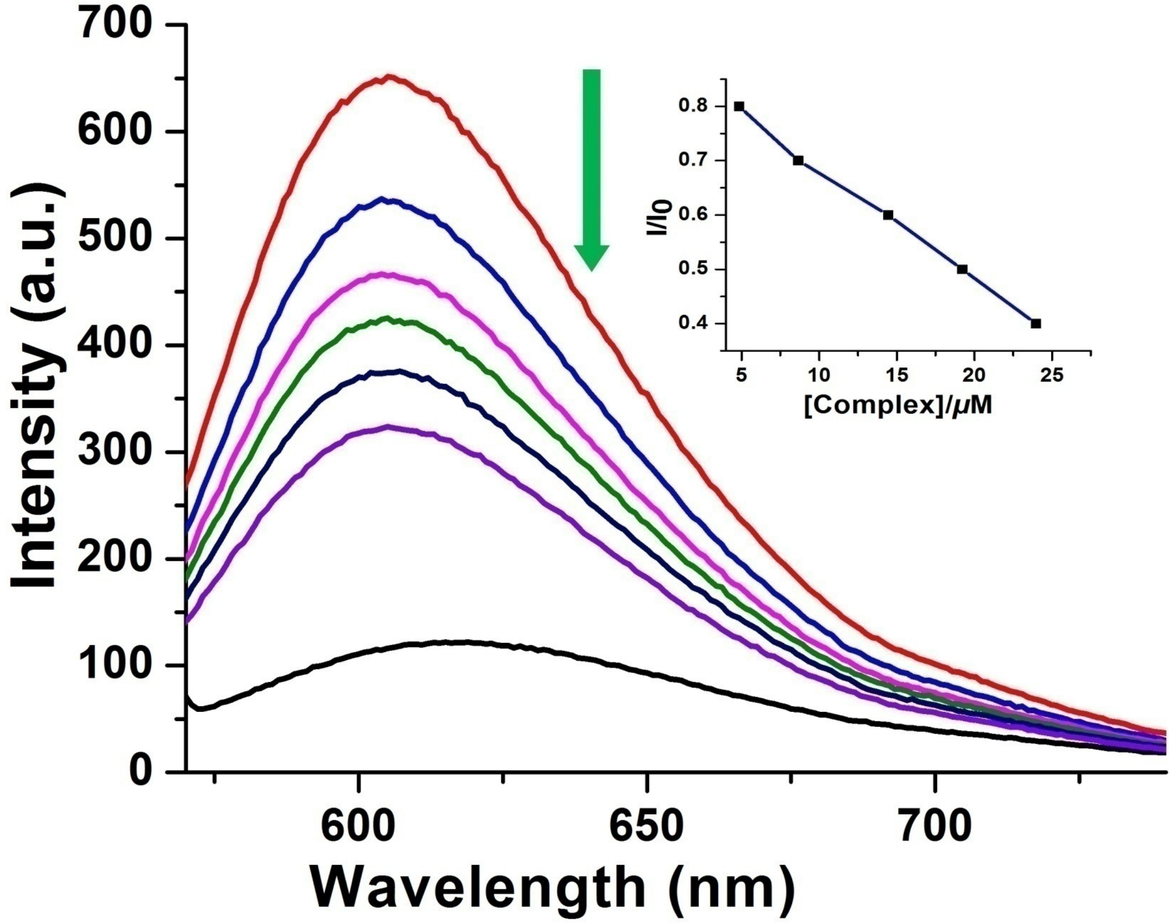

Figure S20. Emission spectral traces of ethidium bromide bound CT-DNA with varying concentration of complex **4** in 5 mM Tris buffer (5 mM Tris- HCl + 5 mM NaCl, pH 7.2) at 25 °C. λ_{ex} = 546 nm, λ_{em} = 603 nm. The inset shows the plot of I/I_0 versus [complex].

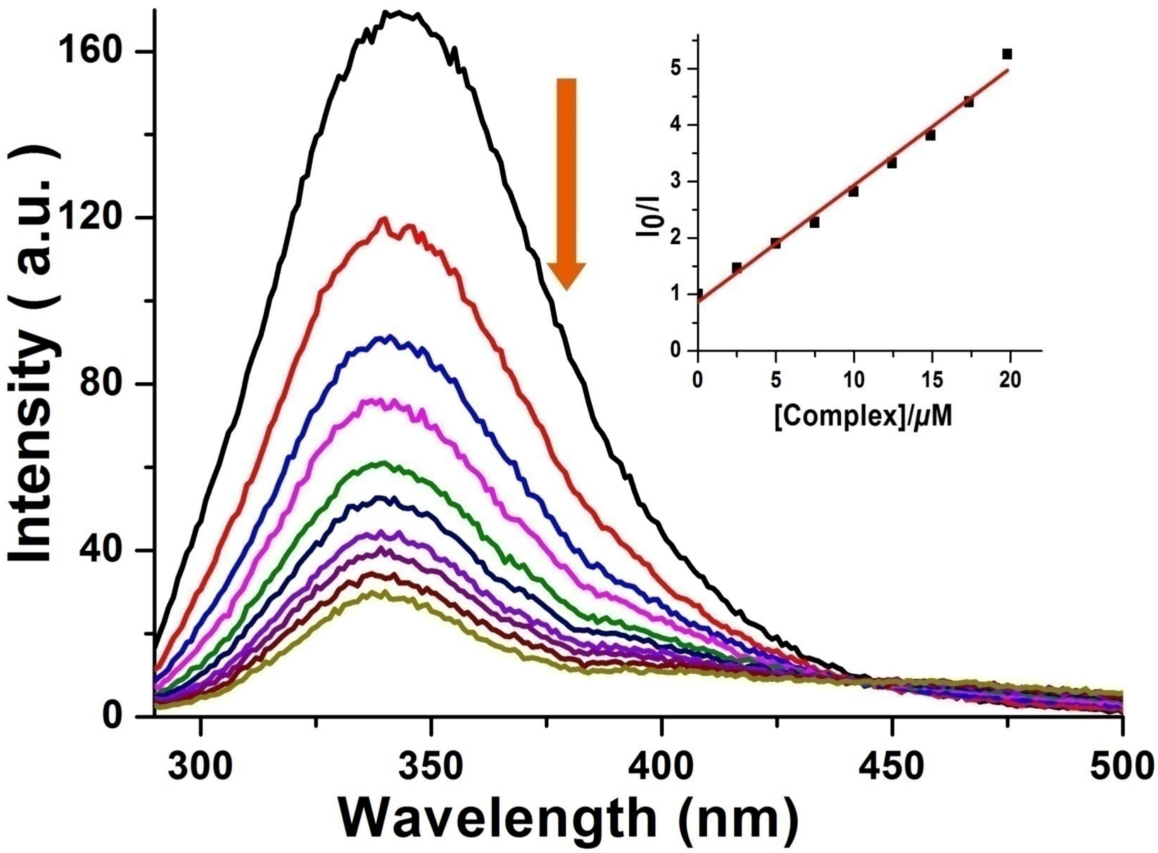

Figure S21. Emission spectral traces of bovine serum albumin (BSA) protein (5 μM) in the presence of complex **2**. The arrow shows the intensity changes on increasing complex concentration. The inset shows the plot of (I_0/I) versus [complex].

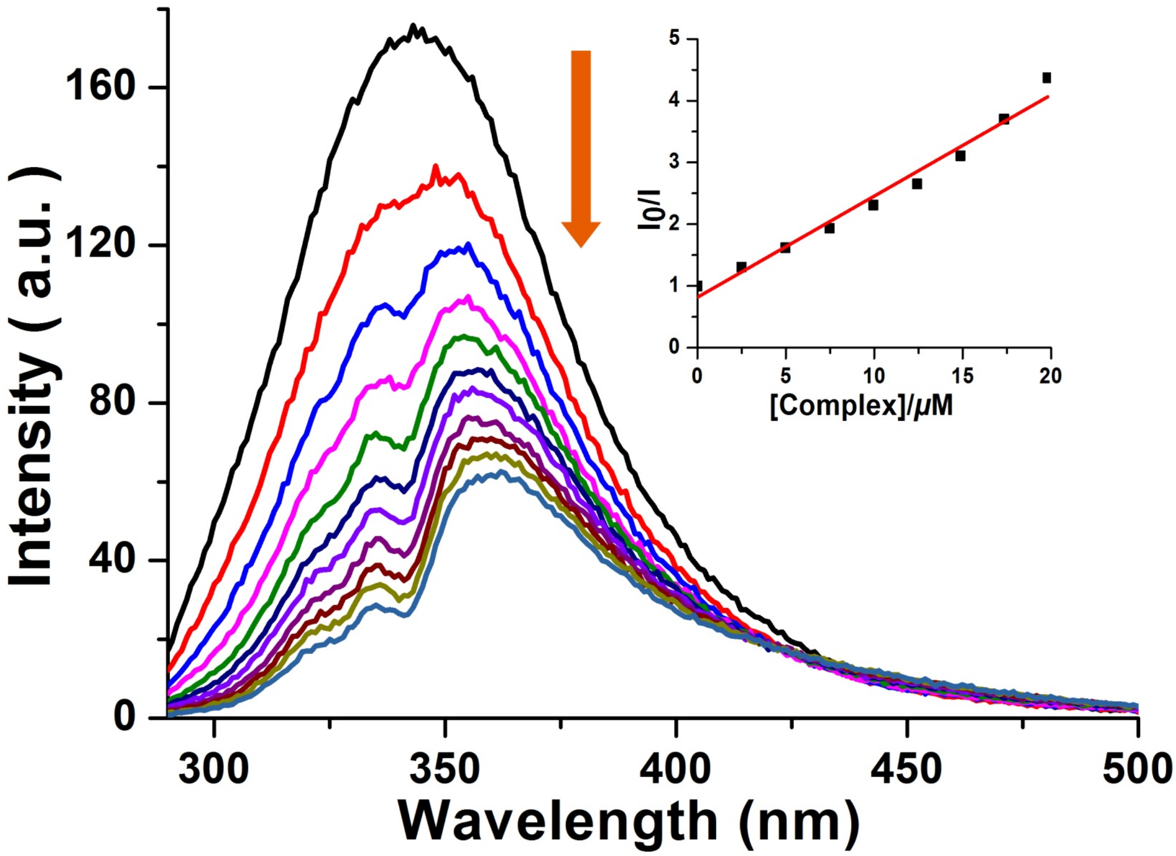

Figure S22. Emission spectral traces of bovine serum albumin (BSA) protein (5 μM) in the presence of complex **3**. The arrow shows the intensity changes on increasing complex concentration. The inset shows the plot of (I_0/I) vs. [complex].

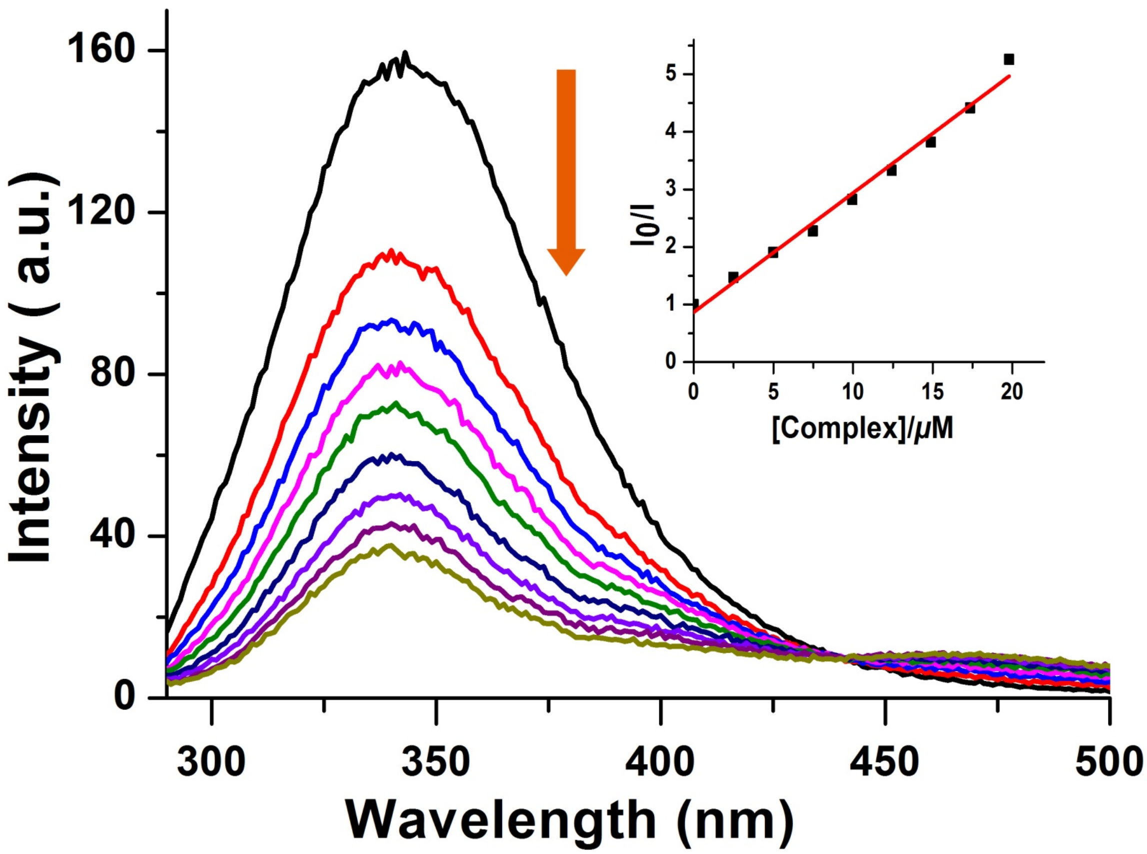

Figure S23. Emission spectral traces of bovine serum albumin (BSA) protein (5 μM) in the presence of complex **4**. The arrow shows the intensity changes on increasing complex concentration. The inset shows the plot of (I_0/I) vs. [complex].

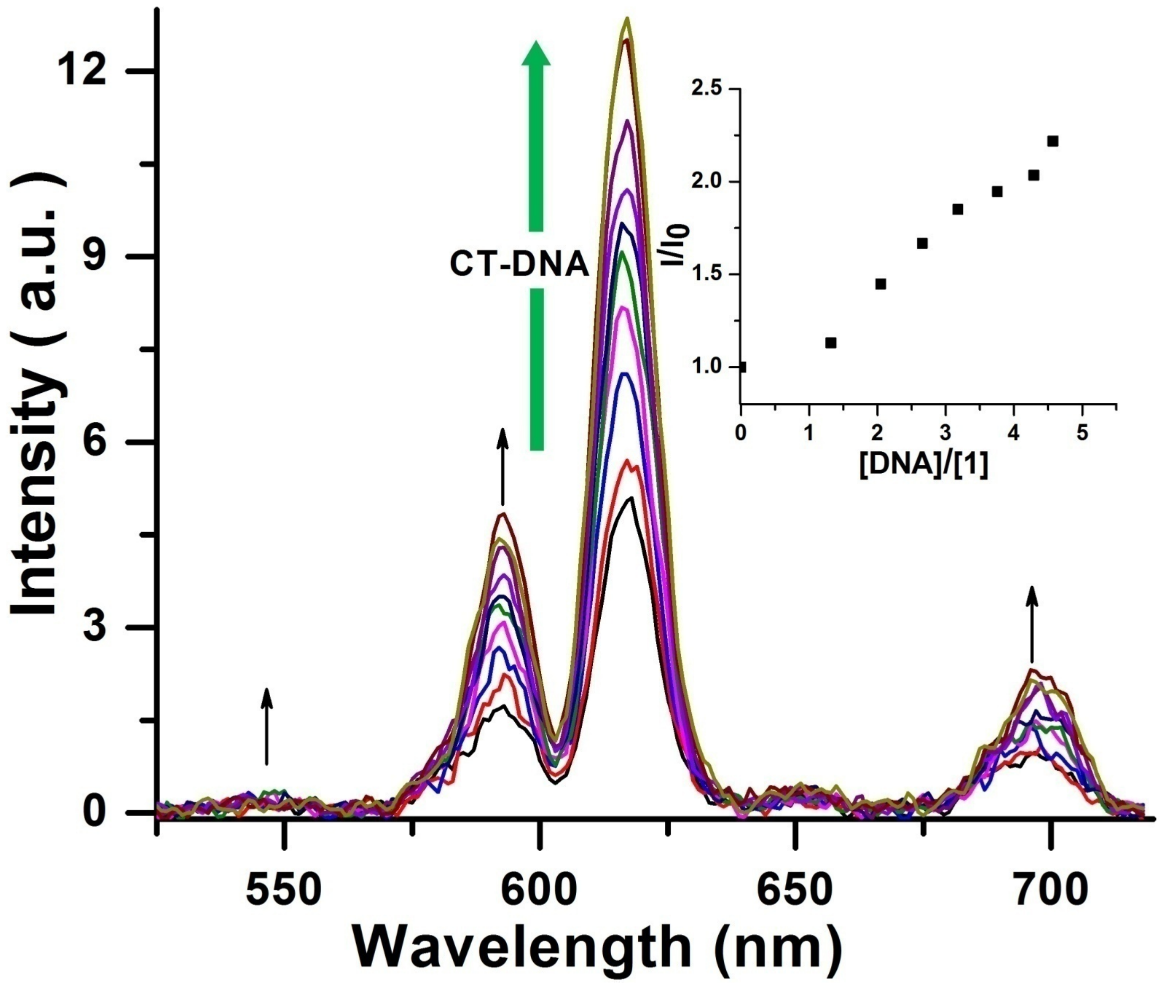

Figure S24. Time-gated emission spectral enhancement of complex **1** upon increasing concentration of CT-DNA in tris- HCl/NaCl buffer (5 mM, pH 7.2) at λ_{ex} = 272 nm (excitation slit width = 10 nm and emission slit width = 10 nm). Inset shows the plot of I/I_0 vs. [DNA]/[**1**].

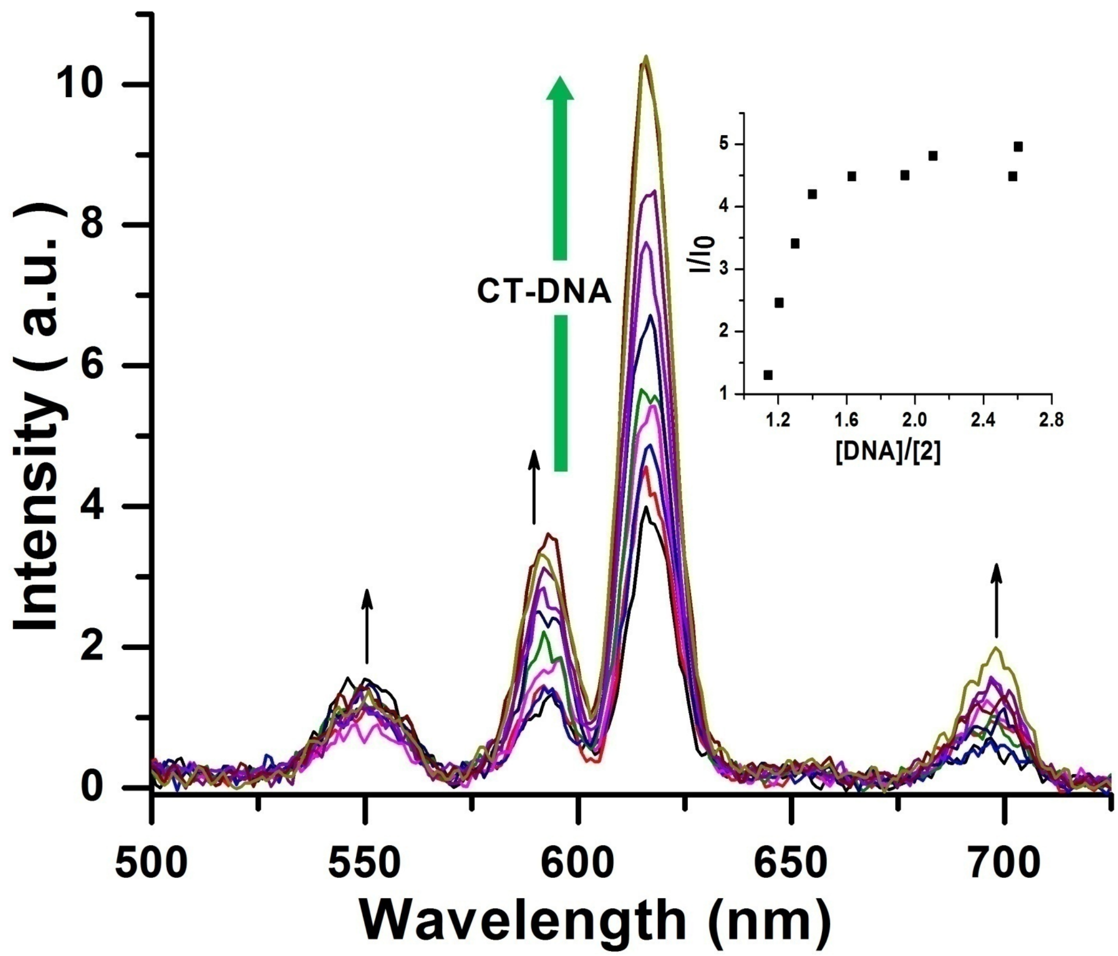

Figure S25. Time-gated emission spectral enhancement of complex **2** upon increasing amount of CT-DNA in 5 mM Tris- HCl/ NaCl buffer (pH 7.2) with λ_{ex} = 272 nm (excitation slit width = 10 nm and emission slit width = 10 nm). Inset shows the plot of I/I_0 vs. [DNA]/[**2**].

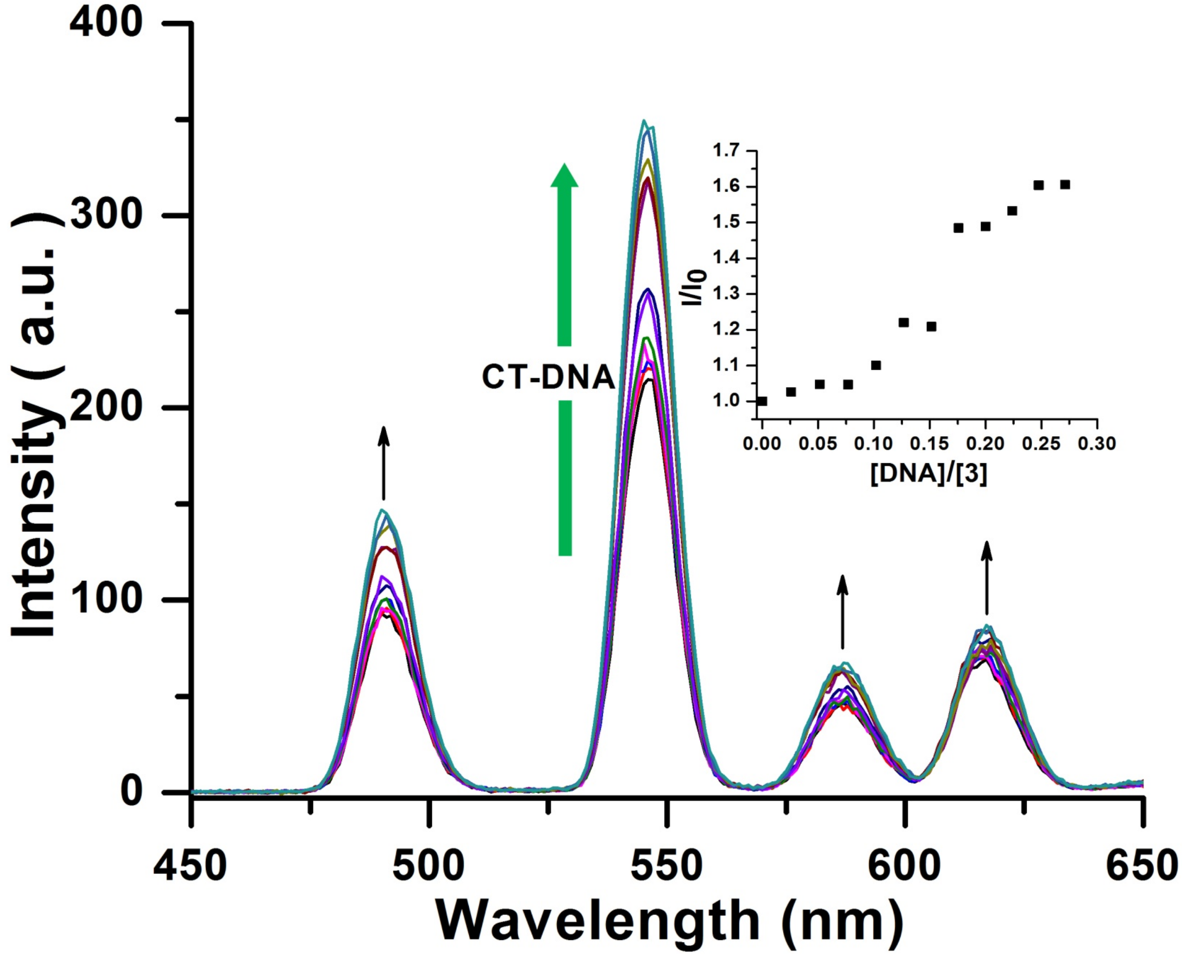

Figure S26. Time-gated emission spectral enhancement of complex **3** upon increasing amount of CT-DNA in Tris-HCl /NaCl buffer (5 mM, pH 7.2) with λ_{ex} = 272 nm (excitation slit width = 10 nm and emission slit width = 10 nm). Inset shows the plot of I/I_0 vs. [DNA]/[**3**].

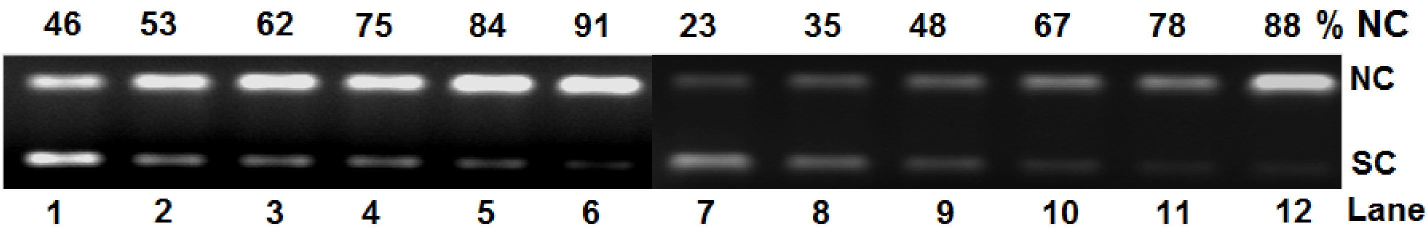

Figure S27. Gel electrophoresis diagram showing the cleavage of SC pUC19 DNA (30 μM, 0.2 μg) incubated with complexes **1** and **2** (10 μM) in 50 mM Tris-HCl/NaCl buffer (pH, 7.2) at 37 ^{0}C for 1 h on irradiation with UV-A light of 365 nm (6 W) at different time. Detailed conditions are given below in a tabular form.

Lane No.	Reaction Condition	λ/nm	Exposure time (t/min)	%NC
1	DNA+ **1**	365	15	46
2	DNA+ **1**	365	30	53
3	DNA+ **1**	365	45	62
4	DNA+ **1**	365	60	75
5	DNA+ **1**	365	90	84
6	DNA+ **1**	365	120	91
7	DNA+ **2**	365	15	23
8	DNA+ **2**	365	30	35
9	DNA+ **2**	365	45	48
10	DNA+ **2**	365	60	67
11	DNA+ **2**	365	90	78
12	DNA+ **2**	365	120	88

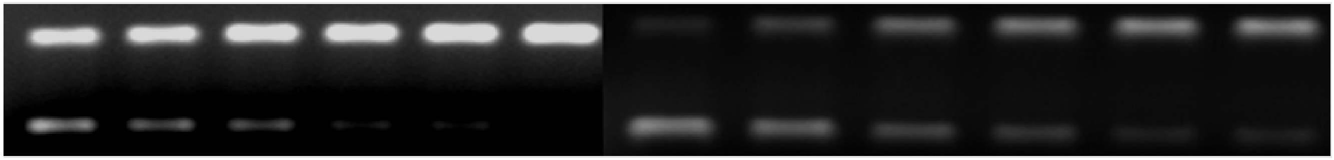

Figure S28. Gel electrophoresis diagram showing the photocleavage of SC pUC19 DNA (30 μM, 0.2 μg) incubated with complexes **3** and **4** (20 μM) in 50 mM Tris-HCl/NaCl buffer (pH, 7.2) at 37 ^{0}C for 2 h on irradiation with UV-A light of 365 nm (6 W) at different time. Detailed conditions are given below in a tabular form.

Lane No.	Reaction Condition	λ/nm	Exposure time (t/min)	%NC
1	DNA+ **3**	365	15	49
2	DNA+ **3**	365	30	58
3	DNA+ **3**	365	45	67
4	DNA+ **3**	365	60	78
5	DNA+ **3**	365	90	88
6	DNA+ **3**	365	120	96
7	DNA+ **4**	365	15	22
8	DNA+ **4**	365	30	37
9	DNA+ **4**	365	45	50
10	DNA+ **4**	365	60	66
11	DNA+ **4**	365	90	77
12	DNA+ **4**	365	120	90

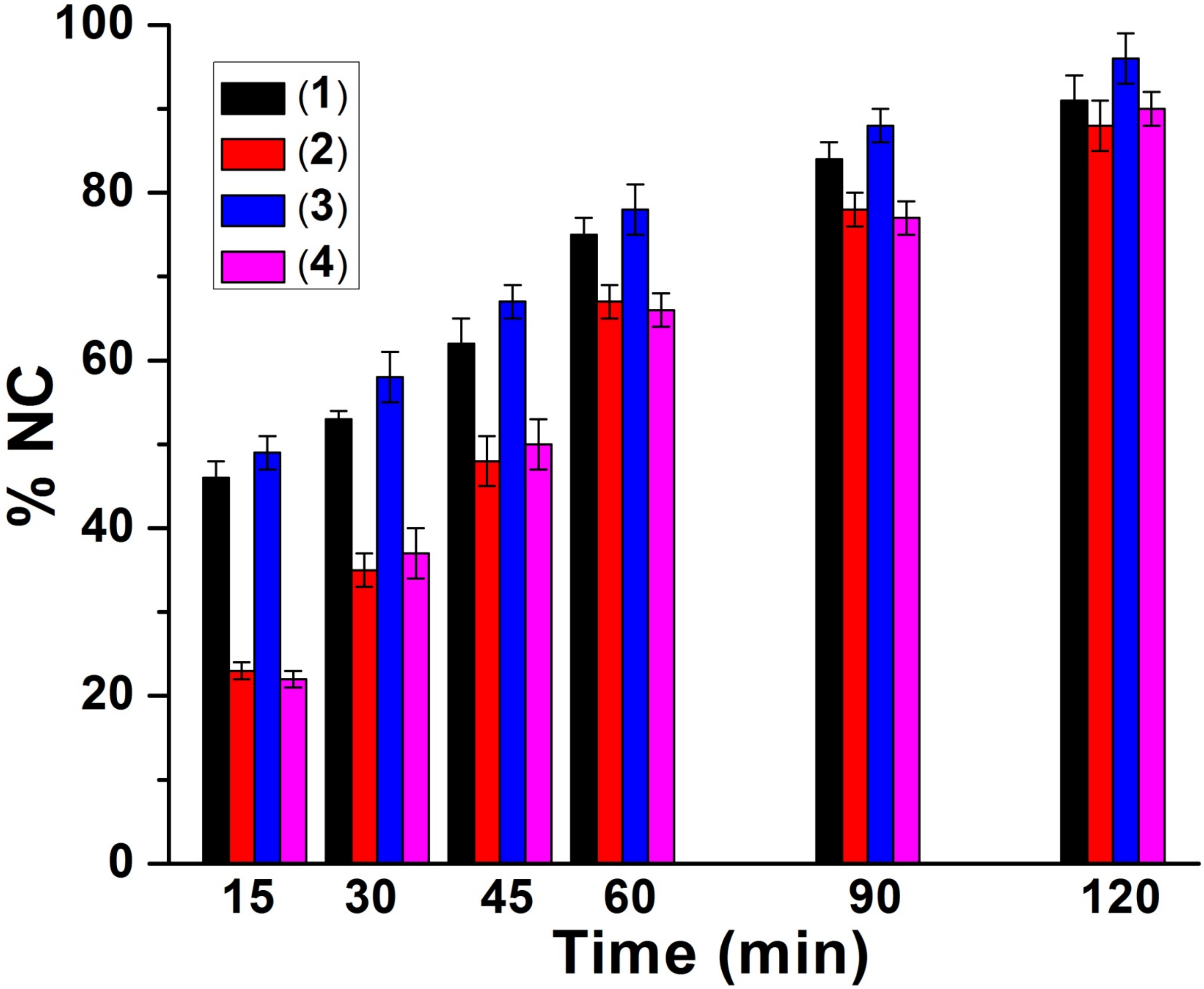

Figure S29. Bar diagram showing the photocleavage of SC pUC19 DNA (30 μM, 0.2 μg) with complexes **1-2** **(**10 μM**)** and **3 - 4** **(**20 μM) in 50 mM Tris-HCl/NaCl buffer (pH, 7.2) on irradiation with UV-A light of 365 nm (6 W) with varying time.

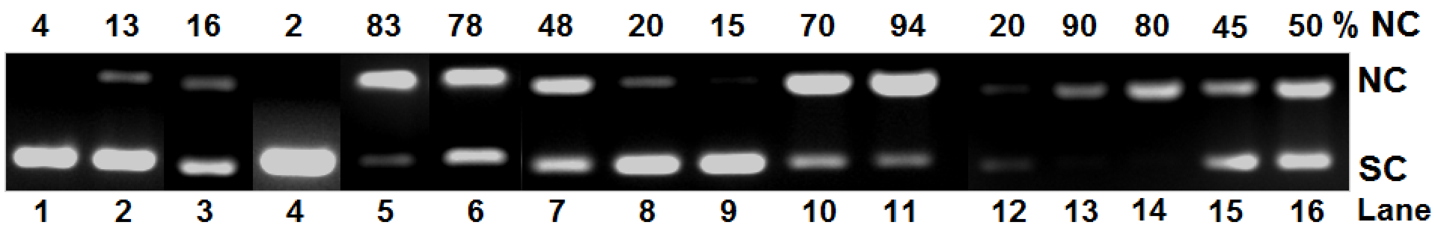

Figure S30. Gel electrophoresis diagram showing the cleavage of SC pUC19 DNA (30 μM, 0.2 μg) incubated with complexes **1** and **2** (10 μM) in 50 mM Tris-HCl/NaCl buffer (pH, 7.2) at 37 ^{0}C for 1 h on irradiation with UV-A light of 365 nm (6 W) for 2 h: lane 1, DNA control; lane 2, DNA + dpq (10 μM); lane 3, DNA + dppz (10 μM); lane 4, DNA + $Eu(NO_3)_3 \cdot 6H_2O$ (10 μM); lane 5, DNA + **1**; lane 6, DNA + **2**; lane 7, DNA + **1** + DMSO (4 μL); lane 8, DNA + **1** + KI (100 μM); lane 9, DNA + **1** + NaN_3 (200 μM); lane 10, DNA + **1** + L-histidine (200 μM); lane 11, DNA + **1** + D_2O (16 μL); lane 12, DNA + methyl green (200 μM); lane 13, DNA + **1** + methyl green (200 μM); lane 14, DNA + **2** + methyl green (200 μM); lane 15, DNA + **1** + catalase (200 μM); lane 16, DNA + **2** + catalase (200 μM).

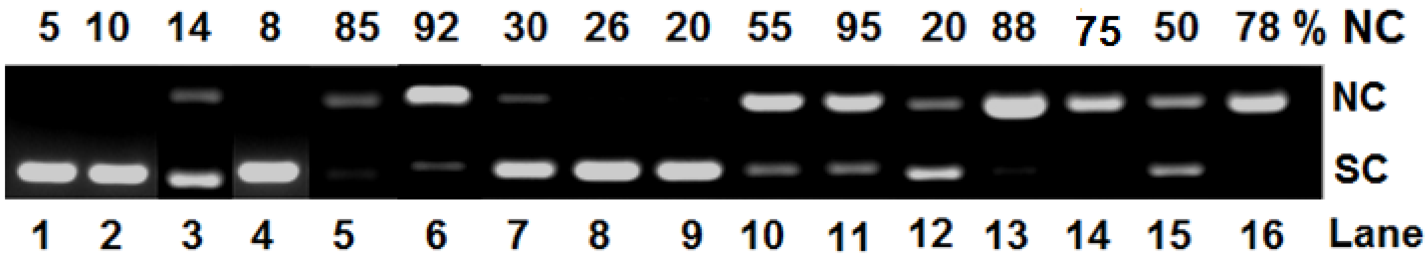

Figure S31. Gel electrophoresis diagram showing the cleavage of SC pUC19 DNA (30 μM, 0.2 μg) incubated with complexes **3** and **4** (20 μM) in 50 mM Tris-HCl/NaCl buffer (pH, 7.2) at 37 ^{0}C for 1 h on irradiation with UV-A light of 365 nm (6 W) for 2 h: lane 1, DNA control; lane 2, DNA + dpq (20 μM); lane 3, DNA + dppz (20 μM); lane 4, DNA + $TbCl_3 \cdot 6H_2O$ (20 μM); lane 5, DNA + **3**; lane 6, DNA + **4**; lane 7, DNA + **3** + DMSO (4 μL); lane 8, DNA + **3** + KI (100 μM); lane 9, DNA + **3** + NaN_3 (200 μM); lane 10, DNA + **3** + L-histidine (200 μM); lane 11, DNA + **3** + D_2O (16 μL); lane 12, DNA + methyl green (200 μM); lane 13, DNA + **3** + methyl green (200 μM); lane 14, DNA + **4** + methyl green (200 μM); lane 15, DNA + **3** + catalase (200 μM); lane 16, DNA + **4** + catalase (200 μM).